APPLIED SCIENCES AND ENGINEERING

N-acetylneuraminate pyruvate lyase controls sialylation of muscle glycoproteins essential for muscle regeneration and function

Afitz Da Silva[1], Junio Dort[1], Zakaria Orfi[1], Xuefang Pan[1], Sjanie Huang[2], Ikhui Kho[1,3], Emilie Heckel[1], Giacomo Muscarnera[1], Patrick Piet van Vliet[1], Luisa Sturiale[4], Angela Messina[4], Donata Agata Romeo[4], Clara D.M. van Karnebeek[5], Xiao-Yan Wen[6], Aleksander Hinek[7], Thomas Molina[1], Gregor Andelfinger[1], Benjamin Ellezam[1], Yojiro Yamanaka[8], Hernando J. Olivos[9], Carlos R. Morales[3], Jean-Sébastien Joyal[1], Dirk J. Lefeber[2,10], Domenico Garozzo[4], Nicolas A. Dumont[1,11]*, Alexey V. Pshezhetsky[1,3]*

Deleterious variants in N-acetylneuraminate pyruvate lyase (NPL) cause skeletal myopathy and cardiac edema in humans and zebrafish, but its physiological role remains unknown. We report generation of mouse models of the disease: Npl^{R63C}, carrying the human p.Arg63Cys variant, and Npl^{del116} with a 116-bp exonic deletion. In both strains, NPL deficiency causes drastic increase in free sialic acid levels, reduction of skeletal muscle force and endurance, slower healing and smaller size of newly formed myofibers after cardiotoxin-induced muscle injury, increased glycolysis, partially impaired mitochondrial function, and aberrant sialylation of dystroglycan and mitochondrial LRP130 protein. NPL-catalyzed degradation of sialic acid in the muscle increases after fasting and injury and in human patient and mouse models with genetic muscle dystrophy, demonstrating that NPL is essential for muscle function and regeneration and serves as a general marker of muscle damage. Oral administration of N-acetylmannosamine rescues skeletal myopathy, as well as mitochondrial and structural abnormalities in Npl^{R63C} mice, suggesting a potential treatment for human patients.

INTRODUCTION

Sialic acids (Sia) constitute a family of negatively charged sugars with a nine-carbon backbone that are found in almost all living organisms. Sia show wide diversity in structures mainly arising from presence of different substitutions in the carbon ring, most common being N-acetylneuraminic acid (Neu5Ac) found in all mammalians, including humans, and N-glycolylneuraminic acid (Neu5Gc) found in nonhuman mammalians. Sia are important components of glycan chains in glycoproteins and glycolipids and are involved in cellular communication, migration, adhesion, tumor cell metastases, and infection processes (1). Sia are cleaved from sialoglycans by sialidases (neuraminidases) followed by recycling of Sia in biosynthesis, or by their degradation into N-acetylmannosamine (ManNAc) and pyruvate by N-acetylneuraminate pyruvate lyase (NPL) (2–4).

Six inherited disorders affecting Sia metabolism have been identified. Three are associated with a decreased free Sia production: GNE myopathy (GNE mutations, Online Mendelian Inheritance in Man (OMIM) 605820), manifesting with the distal muscle weakness leading patients to a wheelchair-bound state (5); spondyloepimetaphyseal dysplasia, Genevieve type (NANS mutations, OMIM 610442), causing severe neurodevelopmental delay and skeletal dysplasia (6); and congenital disorder of glycosylation, type IIf (OMIM 603585), caused by cytidine monophosphate (CMP)–Sia transporter deficiency (SLC35A1 mutations) and presenting with proteinuria, macro-thrombocytopenia, and neurological disease (7–9). The remaining three, associated with increased levels of free Sia, are French-type sialuria (OMIM 269921, GNE mutations), leading to developmental delays (10), and infantile sialic storage/Salla disease (OMIM 269920/604369, SLC17A5 mutations), causing progressive neurologic deterioration and resulting in psychomotor delay, spasticity, athetosis, and epileptic seizures (11). No specific therapies for any of these diseases have been approved yet, highlighting the need of further research in this area (12).

Recently, we have identified a previously unknown inherited disorder of Sia metabolism associated with NPL deficiency. We described two deleterious NPL variants (p.Arg63Cys and p.Asn45Asp) in a compound heterozygous state in a patient who presented with cardiomyopathy, mild skeletal myopathy, and sensorineural hearing loss symptoms. Same variants were present in the proband's older female sibling, who also reported skeletal muscle weakness and limited ability to exercise. Both patients secreted high levels of free Sia in their urine. We further demonstrated that both p.Arg63Cys and p.Asn45Asp variants affected NPL activity in vitro. p.Arg63Cys caused almost complete loss of enzymatic

[1]Department of Pediatrics, Centre Hospitalier Universitaire Sainte-Justine Research Center, University of Montreal, Montreal, QC, Canada. [2]Department of Neurology, Donders Institute for Brain, Cognition, and Behavior, Radboud University Medical Center, Nijmegen 6500, Netherlands. [3]Department of Anatomy and Cell Biology, McGill University, Montreal, QC, Canada. [4]CNR, Institute of Polymers, Composites and Biomaterials, Catania, Italy. [5]Departments of Pediatrics and Human Genetics, Emma Center for Personalized Medicine, Amsterdam Reproduction and Development, Amsterdam University Medical Centers, University of Amsterdam, Amsterdam, Netherlands. [6]Zebrafish Centre for Advanced Drug Discovery and ZebraPeutics (Guangdong) Ltd., HengQin District, Zhuhai, China. [7]Hospital for Sick Children Research Institute, Toronto, ON, Canada. [8]Goodman Cancer Research Centre, McGill University, Montreal, QC, Canada. [9]Waters Corporation, Milford, MA, USA. [10]Translational Metabolic Laboratory, Department of Laboratory Medicine, Radboudumc Institute for Molecular Life Sciences, Radboud University Medical Center, Nijmegen 6500, Netherlands. [11]School of Rehabilitation, University of Montreal, Montreal, QC, Canada.
*Corresponding author. Email: alexei.pchejetski@umontreal.ca (A.V.P.); nicolas.dumont.1@umontreal.ca (N.A.D.)

activity, while the p.Asn45Asp variant retained ~30% of NPL activity (*13*). Zebrafish *npl* knockdown embryos had severe skeletal myopathy and cardiac edema, confirming an essential role of NPL in muscle function (*13*). However, because of the large difference between human and fish biology, generation of a mammalian model is required for better understanding of *NPL* myopathy and development of a therapy.

Here, we describe the first mammalian models of NPL deficiency, a knock-in *Npl*^{R63C} mouse strain carrying the human missense mutation p.Arg63Cys and a knockout *Npl*^{del116} strain with a 116–base pair (bp) exonic deletion in the mouse *Npl* gene. We report that homozygous NPL-deficient mice present skeletal myopathy and delayed muscle regeneration after injury. Both *Npl*^{R63C} and *Npl*^{del116} mice show drastic increase in free Sia in the urine, demonstrating that the enzyme is essential to control levels of this metabolite. We also demonstrate that skeletal myopathy in the *Npl*^{R63C} strain is rescued by treatment with the downstream metabolite of Sia, ManNAc. Together, our results provide new insights into the role of Sia catabolism in mammals and suggest an essential role for NPL in muscle function and regeneration likely via mitochondrial energy production. They also support future evaluation of ManNAc as a potential treatment for *NPL* myopathy in humans.

RESULTS

Homozygous *Npl*^{R63C} and *Npl*^{del116} mice show NPL deficiency in tissues and elevated levels of free Sia in urine

NPL-deficient mouse strains were generated essentially as described (*14*) and genotyped as shown in fig. S1. Genotyping of the offspring from heterozygous crosses revealed a frequency of 23.3% for *Npl*^{R63C} knock-in and 18.75% for *Npl*^{del116} knockout homozygous mutants compatible with the expected Mendelian frequency of 25%. Homozygous *Npl*^{R63C} and *Npl*^{del116} mice, females and males, were fertile and produced normal litter sizes.

Enzymatic NPL activity was measured, as we have previously described (*13*), in the tissues of *Npl*^{R63C} and *Npl*^{del116} mice and their wild-type (WT) counterparts using Neu5Ac as a substrate (Fig. 1A). In WT mice, the highest levels of NPL activity were detected in the intestine (80 nmol hour mg^{-1}), followed by the kidney, spleen, and stomach. Considerable NPL activity (20 to 25 nmol hour mg^{-1}) was also detected in skeletal muscles, lungs, and brain, whereas, in the liver and heart, activity levels were below 10 nmol hour mg^{-1}. In all studied tissues of homozygous *Npl*^{R63C} and *Npl*^{del116} mice, NPL activity was reduced to background levels, consistent with our previous report on the deleterious character of the R63C change in the human protein (*13*). In contrast, *Npl* mRNA levels were drastically different in the knockout and knock-in mice: While mRNA levels measured by real-time quantitative polymerase chain reaction (qPCR) in kidney tissues of homozygous *Npl*^{R63C} and WT mice were similar, the *Npl* transcript could not be detected in homozygous *Npl*^{del116} mice (Fig. 1B). To analyze NPL protein levels by immunoblot, we used kidney tissues, where the enzyme shows one of the highest expression levels. A presence of a 36-kDa NPL cross-reacting protein band was detected in tissues of WT animals but not in both mutant strains (Fig. 1C). These results, together with our previous data obtained in human embryonic kidney (HEK) 293 cells overexpressing human R63C mutant NPL variant (*13*), were consistent with the suggestion that the *Npl*^{del116} transcript is degraded by the nonsense-mediated decay process, whereas the *Npl*^{R63C}

transcript produces unstable mutant protein. Independently of the mechanism, NPL enzyme activity is reduced to the background level in tissues of both mice.

Substantially elevated levels of free Sia were detected in urine of the human patient carrying the R63C NPL variant (*13*). To test whether sialuria was recapitulated in the mouse models, we measured the concentration of free total Sia in the urine and found that both *Npl*^{R63C} and *Npl*^{del116} mice showed a notable increase of free Sia levels (Fig. 1D).

Homozygous NPL-deficient mice demonstrate skeletal muscle weakness but normal heart development and function

The gross phenotypic appearance of homozygous *Npl*^{del116} and *Npl*^{R63C} mice was indistinguishable from their normal littermates. They also showed a normal behavior in Y-maze test, suggestive of a normal cognitive ability at 4 months of age (fig. S2). General examination and microscopic analysis of organs and tissues with detectable NPL expression, including colon, kidney, stomach, spleen, skeletal muscles, brain, lungs, liver, and heart, also did not reveal obvious pathological changes. Nevertheless, since myopathy and cardiomyopathy are the two major clinical features of the human patients, we have further analyzed skeletal muscle and heart function in NPL-deficient mouse strains. This analysis revealed an early-onset muscle weakness in several neuromuscular tests in both strains (Fig. 2). In particular, animals have shown significantly reduced latency to fall in the hindlimb and front limb suspension tests performed at the ages of 10 days and 6 weeks, respectively (Fig. 2, A and B), suggesting reduced muscle strength, increased fatigue, and/or low endurance. Reduction of muscle strength was confirmed by the results of grip strength test conducted at 10 weeks (Fig. 2C) and the measurements of isometric contractile properties of the extensor digitorum longus (EDL) muscle ex vivo (Fig. 2, D and E). The latter test directly demonstrated a significant reduction of the maximum tetanic force and specific force for *Npl*^{del116} and *Npl*^{R63C} mice compared to WT mice. After repeated contractions (60 stimulations), EDL muscles from *Npl*^{del116} showed increased fatigue compared to WT and muscles from *Npl*^{R63C} mice, a trend toward higher fatigue (Fig. 2F). At the same time, muscle mass measured as a ratio of quadriceps, triceps, gastrocnemius, and tibialis anterior muscle mass to the body mass was similar in *Npl*^{del116} and *Npl*^{R63C} mice and their WT counterparts (Fig. 2G). All mice also showed a normal body mass gain (Fig. 2H). The quantification of fiber diameters of quadriceps muscle showed a shift toward somewhat smaller diameter size in *Npl*^{del116} and *Npl*^{R63C} mice (significant reduction of the fibers with a 50 to 60 μm diameter) compared to WT mice (Fig. 2I).

In contrast, unlike the human patient and *npl*-deficient zebrafish embryos (*13*), the *Npl*^{R63C} mice presented normal heart development and function (fig. S3). Heart mass normalized to body mass, measured at the age of 7 months, was similar in *Npl*^{R63C} mice and their WT counterparts (fig. S3A). The heart rate, left ventricular ejection fraction (LVEF), left ventricular end-diastolic dimension (LVEDD), and left ventricular end-systolic dimension (LVESD), measured by echocardiography in *Npl*^{R63C} mice, although showing a trend to reduction, were not significantly different from those in the WT mice (fig. S3, B to E). Since the NPL protein and activity were equally reduced in the knock-in and knockout strains, the heart function has not been studied in *Npl*^{del116} mice.
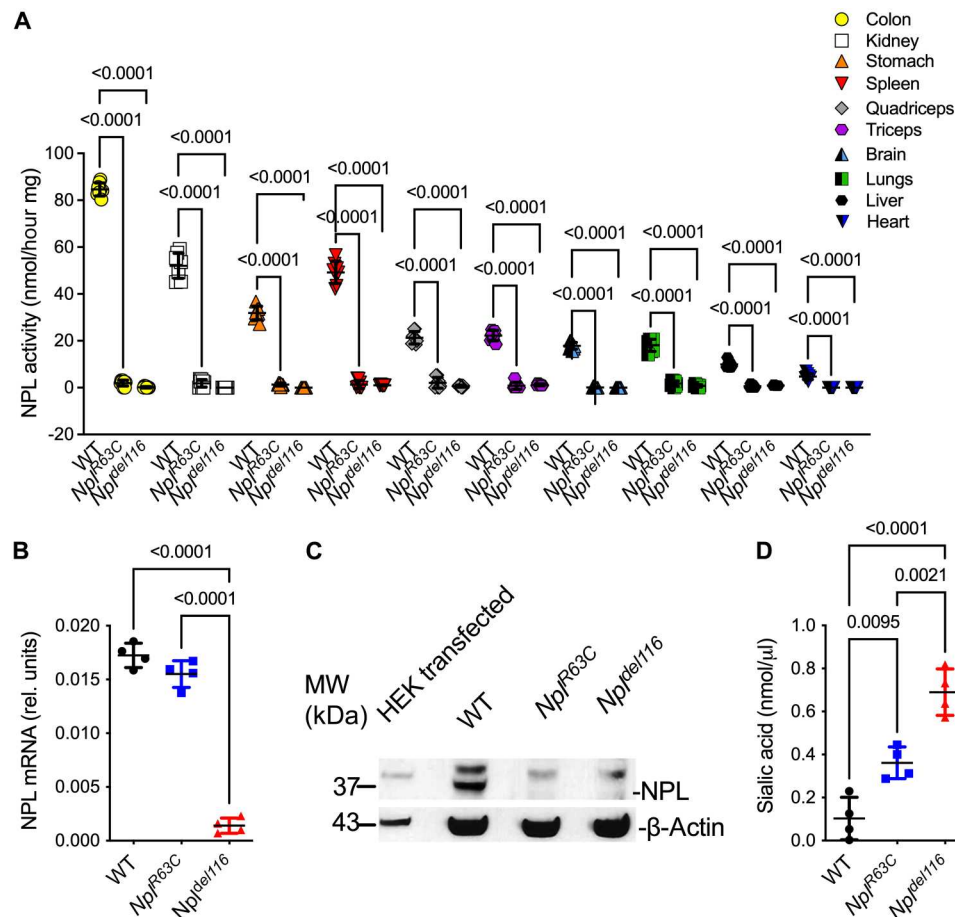
Fig. 1. Homozygous _Npl^R63C_ and _Npl^del116_ mice show NPL deficiency in tissues and massive urinary excretion of free Sia. (**A**) NPL activity in homogenates of skeletal muscles, visceral organs, and brain of _Npl^R63C_, _Npl^del116_, and WT mice. (**B**) Relative _Npl_ mRNA levels in kidney of _Npl^R63C_, _Npl^del116_, and WT mice. Four mice (two males/two females) were analyzed for each group. Statistical analyses were performed using a one-way analysis of variance (ANOVA) with Tukey post hoc test. (**C**) Western blot of mouse kidney tissues showing an absence of 36-kDa NPL cross-reacting protein band in both _Npl^R63C_ and _Npl^del116_ mice. A lysate of HEK cells transfected with a plasmid expressing WT human FLAG-(DYKDDDDK)–tagged NPL [molecular weight (MW), 37 kDa] was used as a positive control. Bottom panel shows a loading control, β-actin. (**D**) Total free Sia concentration in the urine of WT, _NPL^R63C_, and _NPL^del116_ mice. Four mice (two males/two females) were analyzed for each group. Statistical analyses were performed using a one-way ANOVA with Tukey post hoc test.

Npl^R63C mice show slower healing and smaller myofibers after cardiotoxin-induced muscle injury

Since the reduced myofiber size and muscle strength in NPL-deficient mice could potentially implicate alterations in muscle regeneration, we analyzed formation of new muscle fibers during muscle healing after cardiotoxin-induced injury. For this experiment, we have selected the knock-in _Npl^R63C_ strain, since the results obtained with this model could be directly translated to human patients with the same molecular defect. Intramuscular injections of cardiotoxin were performed into the right tibialis anterior muscle under general anesthesia. The muscles were harvested 14 and 21 days after injury (i.e., at the stages of myofiber formation/maturation and return to homeostasis, respectively) and cut cross-sectionally to quantify diameter of newly formed fibers, number of central nuclei per fiber, and the number of myogenin-positive cells. Assessment of histological changes in skeletal muscles at 14 and 21 days into the regeneration process showed that healing was more advanced in WT than in _Npl^R63C_ mice, which still had a strong regeneration deficit at 21 days after injury (Fig. 3A). At 21 days after injury, the diameters of

newly formed fibers in _Npl^R63C_ mice were smaller compared with those in WT mice (Fig. 3, B and C). Fourteen days after cardiotoxin injection, the number of myogenin-positive cells in muscles of _Npl^R63C_ mice was significantly reduced compared to WT, indicating that most myogenic precursor cells lacked proper differentiation potential (Fig. 3, D and E).

ManNAc therapy rescues muscle weakness and muscle regeneration defects in _Npl^R63C_ mouse model

Previously, we were able to demonstrate the rescue of the heart and muscle phenotype in _npl_-deficient zebrafish embryos by treatment with metabolites downstream of the NPL-catalyzed reaction, with ManNAc showing the highest activity (_13_). We, thus, decided to test whether this compound could also rescue muscle weakness in NPL-deficient mice. _Npl^R63C_ breeding pairs were administered water or water supplemented with ManNAc [5 mg/ml; ~1.0 g kg^{-1} body weight (BW) day^{-1}]. The treatment continued for the nursing females as well as for the offspring after weaning and until the time of analysis. At this dose, ManNAc was well tolerated
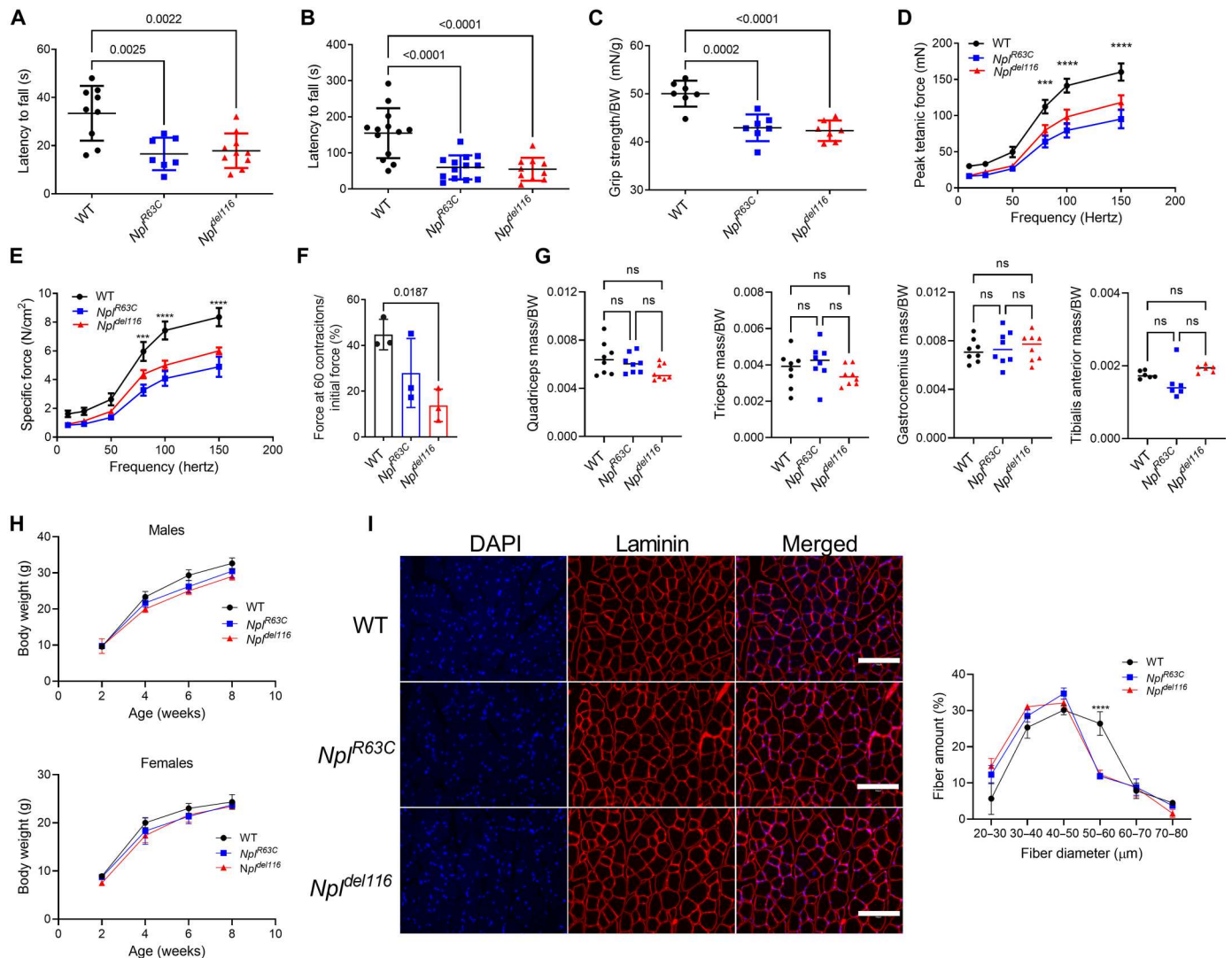
Fig. 2. Homozygous *Npl^R63C* and *Npl^del116* mice display a muscle weakness. (**A**) Hindlimb suspension test with WT (*n* = 9, 5 males and 4 females), *Npl^R63C* (*n* = 7, 4 males and 3 females), and *Npl^del116* (*n* = 10, 5 males and 5 females) 10-day-old mice. (**B**) Front limb suspension test with WT (*n* = 13, 8 males/5 females), *Npl^R63C* (*n* = 13, 7 males/6 females), and *Npl^del116* (*n* = 10, 5 males and 5 females) 6-week-old mice. (**C**) Grip strength test with WT (*n* = 7, 4 males and 3 females), *Npl^R63C* (*n* = 7, 4 males and 3 females), and *Npl^del116* (*n* = 3, 3 males/4 females) 10-week-old mice. All statistical analyses were performed using a one-way ANOVA test with Tukey post hoc test. Isometric contractile properties of EDL muscles shown as specific force (**D**) and maximum force (**E**) in 2-month-old WT, *Npl^del116*, and *Npl^R63C* mice. Data are presented as means ± SEM of *n* = 6 (3 males and 3 females) mice for each group. Statistical analysis was performed using a two-way ANOVA test with a Bonferroni post hoc test, ***P < 0.001, ****P < 0.0001. ns, not significant. (**F**) Ex vivo isometric fatigue characteristics of EDL muscle from WT, *Npl^del116*, and *Npl^R63C* mice. Bar graph shows percent of initial force produced after 60 contractions. (**G**) Mass of quadriceps, triceps, gastrocnemius, and tibialis anterior muscles is normal in 2-month-old WT, *Npl^R63C*, and *Npl^del116* mice (*n* = 6, 3 males and 3 females for each genotype). (**H**) *Npl^del116* and *Npl^R63C* mice show normal body mass gain (*n* = 4 per sex per genotype). (**I**) Distribution of myofiber diameters in 2-month-old WT, *Npl^R63C*, and *Npl^del116* mice. Diameters of myofibers were quantified by morphometric analysis of quadriceps sections, labeled for laminin (red), from WT, *Npl^del116*, and *Npl^R63C* mice using ImageJ; *n* = 3 per sex per genotype. Scale bar, 150 μm. Statistical analyses were performed using two-way ANOVA test with a Bonferroni post hoc test, ****P < 0.0001.

by mice, and no side effects that could be potentially attributed to the treatment were detected. Muscle strength was measured by hindlimb suspension test at postnatal day 10, front limb suspension test at 6 weeks, and grip test at 10 weeks of age. The maximum tetanic force and specific force of the EDL muscle was also measured at the age of 10 weeks (Fig. 4, A to E). In all four functional tests, the treated *Npl^R63C* mice showed a performance similar or close to that of WT mice. In contrast, no significant improvement of

muscle strength was observed in *Npl^R63C* mice treated with the lower ManNAc dose (1 mg/ml; ~0.2 g kg⁻¹ BW day⁻¹) (Fig. 4A).

Six-week-old *Npl^R63C* mice, treated since birth with ManNAc (1.0 g kg⁻¹ BW day⁻¹), retained normal muscle strength, as measured by the front limb suspension test 24 hours after being withdrawn from the drug (Fig. 4B), suggesting that the treatment restores structural defects in the muscle rather than provides an acute metabolic compensation. To verify this, ultrastructural organization of muscle fibers in WT, *Npl^R63C*, and ManNAc-treated
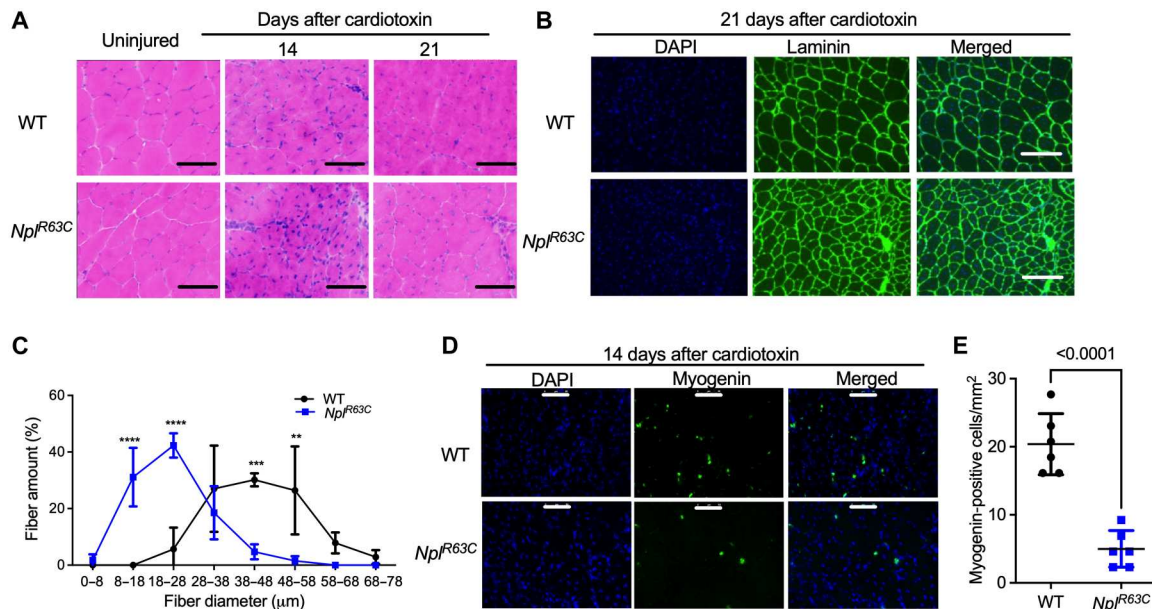
Fig. 3. Npl^{R63C} mice show slower healing and produce myofibers with smaller diameter after cardiotoxin-induced muscle injury. (**A**) Histological changes in tibialis anterior muscle on the 14th and 21st days of regeneration after intramuscular cardiotoxin injection. Panels show representative mouse muscle cross sections after hematoxylin and eosin (H&E) staining. Scale bar, 150 μm. Three WT and three Npl^{R63C} mice (two males, one female) were analyzed. (**B**) Representative tibialis anterior sections from injured WT and Npl^{R63C} mice 21 days after injury, labeled with 4′,6-diamidino-2-phenylindole (DAPI, blue) and anti-laminin antibody (green). Scale bar, 150 μm. (**C**) Distribution of myofiber diameters in injured WT and Npl^{R63C} mice 21 days after injury. Diameters of myofibers were quantified by morphometric analysis of tibialis anterior sections from three WT and three Npl^{R63C} mice (two males/one female) using ImageJ software. Statistical analyses were performed using two-way ANOVA test; **P < 0.01, ***P < 0.001, and ****P < 0.0001. (**D**) Representative tibialis anterior sections from three WT and three Npl^{R63C} mice (two males/one female) 14 days after injury labeled with DAPI (blue) and anti-myogenin antibody (green). Scale bar, 50 μm. (**E**) Density of myogenin⁺ cells/mm² in three WT and three Npl^{R63C} mice (two males/one female). Quantifications were performed using three sections per mouse. Statistical analysis was performed using Student's t test, P < 0.0001.

Npl^{R63C} mice was further studied by transmission electron microscopy (TEM) (Fig. 4, F to H). In the tissues from Npl^{R63C} mice, branched fibers and nonspecific myopathic signs (Fig. 4F), nondetectable in WT or ManNAc-treated Npl^{R63C} mice, were observed. Besides, the myofibers from Npl^{R63C} mice had irregular shapes and, in general, were smaller than those in the muscles of WT animals (Fig. 4F). Notably, myocytes from the Npl^{R63C} mice contained more mitochondria with vacuoles and showed accumulation of lysosomes and distended Golgi cisterna, which were still regularly located between the parallelly oriented cytoskeletal fibers and did not disturb the cellular shape (Fig. 4, G and H). Most of the myocytes from Npl^{R63C} mice also contained glycogen aggregates. In contrast, the myocytes from ManNAc-treated Npl^{R63C} mice had evenly sized and shaped fibers and mitochondria with more developed cristae, resembling those from WT mice (Fig. 4, G and H). Myocytes of Npl^{del116} mice showed defects similar to those in Npl^{R63C} mice, confirming that they are associated with NPL deficiency (Fig. 4, F to H).

To test whether ManNAc also rescued defects in muscle regeneration after cardiotoxin injury, we studied the muscle healing in Npl^{R63C} mice undergoing treatment with ManNAc (5 mg/ml). Our data demonstrate that at 14 and 21 days into the regeneration process, the healing process was drastically accelerated in Npl^{R63C} mice receiving ManNAc compared with untreated mice (Fig. 5A). In addition, at 21 days after injury, alterations in the diameter of newly formed fibers in Npl^{R63C} mice were rescued by ManNAc (Fig. 5, B and C). To elucidate the mechanism underlying delayed regeneration of muscle after cardiotoxin injury, we studied

proliferation of myoblasts derived from the muscles of WT, Npl^{R63C}, and Npl^{del116} mice, their fusion into myotubes, and maturation in vitro (Fig. 5D). The experiments were conducted in the absence and in the presence of 800 μM ManNAc in the differentiation medium. While proliferation of myoblasts was similar for all cultures (not shown), on day 5 of differentiation, we observed a significant reduction in the number of nuclei per myotube in the cells from both Npl^{R63C} and Npl^{del116} mice, suggestive of reduced ability of myoblasts to fuse (Fig. 5D). We also observed a significant reduction in the diameter of myosin-positive myotubes for the cells derived from NPL-deficient mice, suggesting that NPL deficiency also interferes with maturation of myotubes. The reduction in myotube diameter in the cells from Npl^{R63C} mice was rescued by addition of ManNAc to the culture medium (Fig. 5D). Together, our results provide evidence that muscle deficiency in NPL-deficient mice is associated with defects in myofiber maturation and organization, and that these defects are rescued by ManNAc.

Metabolomic and glycomic profiling of muscle tissues of NPL-deficient mice reveals alterations in protein sialylation reversed by ManNAc treatment

To get insight into the molecular mechanisms underlying the muscular weakness in NPL-deficient mice and its rescue by ManNAc, we conducted the analysis of soluble metabolites extracted from quadriceps tissues of 2-month-old WT, Npl^{del116}, and Npl^{R63C} mice as well as of Npl^{R63C} mice treated from utero with ManNAc. Three animals were analyzed for each group. Metabolites were extracted with methanol/water (1:1) mixture, analyzed with reversed-
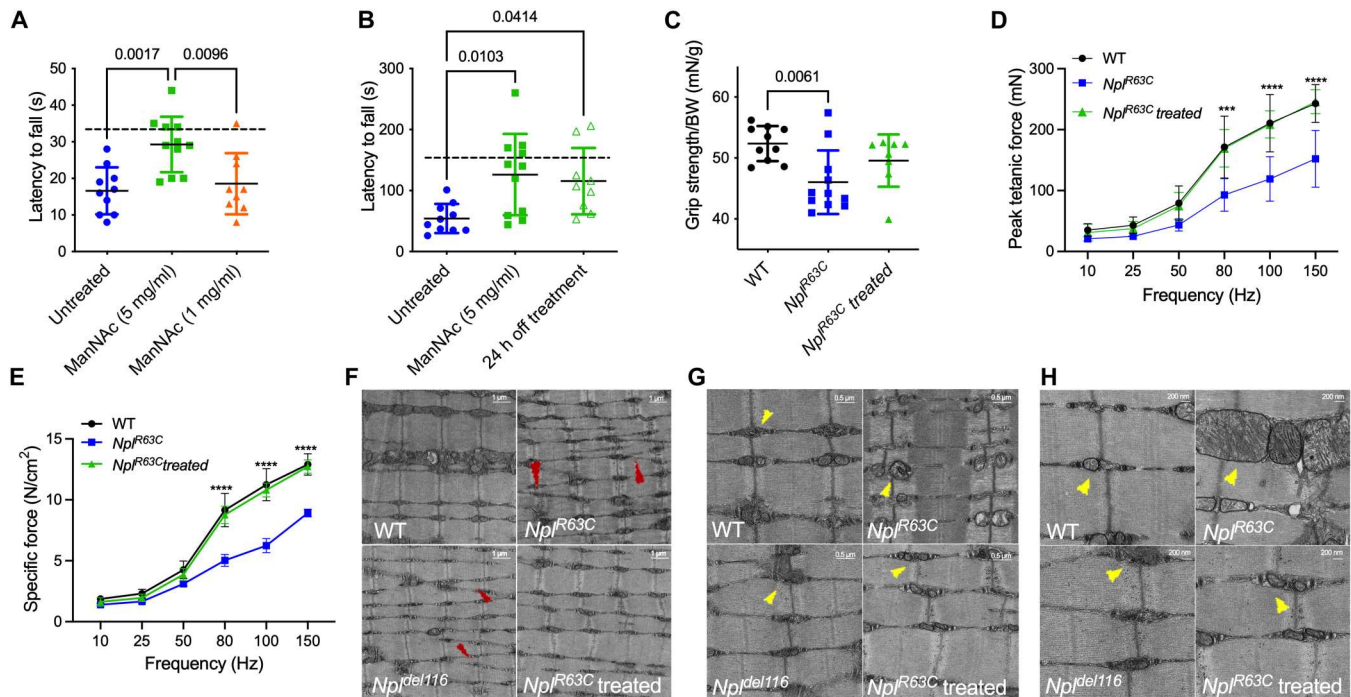
Fig. 4. ManNAc treatment rescues muscle weakness and accelerates muscle injury healing in NPL-deficient *Npl^del116* mice. (**A**) Latency to fall in hindlimb suspension test performed on 10-day-old untreated *Npl^R63C* mice (*n* = 10, 5 males/5 females) and those receiving ManNAc (*n* = 11, 6 males/5 females). Statistical analysis was performed using ANOVA test with a Tukey post hoc test. (**B**) Latency to fall in front limb suspension test performed on 6-week-old untreated (*n* = 10, 5 males/5 females) and ManNAc-treated (*n* = 11, 6 males/5 females) *Npl^R63C* mice during the treatment and 24 hours after discontinuation of the treatment. Statistical analysis was performed using ANOVA test with a Tukey post hoc test. (**C**) Grip strength in 10-week-old WT (*n* = 10, 5 males/5 females), untreated *Npl^R63C* (*n* = 11, 5 males/6 females), and ManNAc-treated *Npl^R63C* mice (*n* = 8, 4 males/4 females). Data are presented as the mean force normalized to body mass. Statistical analysis was performed using ANOVA test with a Tukey post hoc test. Isometric contractile properties of EDL muscles shown as maximum force (**D**) and specific force (**E**) in 2-month-old WT, *Npl^R63C*, and *Npl^R63C* mice treated with ManNAc. Data are presented as means ± SEM (*n* = 5, 3 males/2 females per group). Statistical analyses were performed using a two-way ANOVA test with a Bonferroni post hoc test; ***$P < 0.001$ and ****$P < 0.0001$. Transmission electronic images with magnification ×4800 (**F**), ×9300 (**G**), and ×13,000 (**H**) of tibialis anterior muscle longitudinal sections from WT, *Npl^R63C*, *Npl^del116*, and ManNAc-treated *Npl^R63C* mice. Red arrowheads show irregularly shaped myotubes and yellow arrowheads show dysmorphic mitochondria in muscles of NPL-deficient mice. Panels show representative results from four mice (two males/two females) per group.

phase ultraperformance liquid chromatography–tandem mass spectrometry (UPLC-MS/MS), as described (*15*), quantified by integration of areas under chromatograms, and compared using Progenesis QI software. All data were normalized and compared to those obtained with pulled extracts (fig. S4). Metabolites, where levels were significantly different between the groups, were identified using Progenesis QI software.

We found that concentrations of Sia-nucleotides, CMP-Neu5Ac, and CMP-Neu5Gc, involved in the synthesis of glycans, showed a trend toward an increase in both *Npl^del116* and *Npl^R63C* mice compared to WT, while CMP-Neu5Gc levels in *Npl^R63C* mice receiving ManNAc treatment were similar to those in the WT animals (fig. S5). To verify these results, we performed a targeted quantitative analysis of Sia in urine and muscle tissues as well as Sia-nucleotides in muscle tissues of WT, *Npl^del116*, *Npl^R63C*, and ManNAc-treated *Npl^R63C* mice. In muscles, both Neu5Ac and Neu5Gc were significantly increased in *Npl^del116* and *Npl^R63C* mice compared to WT (Fig. 6, A and B), but Neu5Gc showed, on average, a much higher increase (8-fold for *Npl^R63C* and 12-fold for *Npl^del116* mice) compared with Neu5Ac (2.8-fold for *Npl^R63C* and 2.6-fold for *Npl^del116*). Similar results were obtained for the urine (Fig. 6, E to G). CMP-Neu5Ac in the muscle was not significantly increased, but CMP-Neu5Gc was significantly increased (1.6-fold in the

Npl^R63C mice and 2.2-fold in the *Npl^del116* mice). ManNAc treatment, in general, did not affect Sia or CMP-Sia levels in the muscle but significantly increased levels of total Sia (Fig. 6E) and Neu5Ac (Fig. 6F) in the urine. In contrast, the levels of Neu5Gc in the urine of ManNAc-treated *Npl^R63C* mice showed a trend toward decrease compared with untreated *Npl^R63C* mice and were not significantly different from those in the WT mice (Fig. 6G).

Since increased levels of Neu5Gc could potentially cause alterations in the synthesis of glycans, including complex glycans of glycoproteins, we performed analysis of *N*-glycomes in muscle tissues of WT, *Npl^R63C*, and ManNAc-treated *Npl^R63C* mice. Matrix-assisted laser desorption/ionization (MALDI)–time-of-flight (TOF) MS profiles of the permethylated *N*-glycan pool derived from protein fractions consisted mainly of paucimannose and oligomannose structures. Hybrid and complex species were also present, as both nonfucosylated and core-fucosylated forms. Complex glycans were mainly biantennary and, in a minor part, triantennary, with most of the antennary epitopes terminated by Neu5Ac or Neu5Gc, the latter being more abundant. Asialo-glycoforms bearing Gal-GlcNAc and Gal-Gal branches were present to a lesser extent (Fig. 7A and table S1).

In *Npl^R63C* mice, changes in the relative intensities of glycan families were observed compared to WT and ManNAc-treated *Npl^R63C*
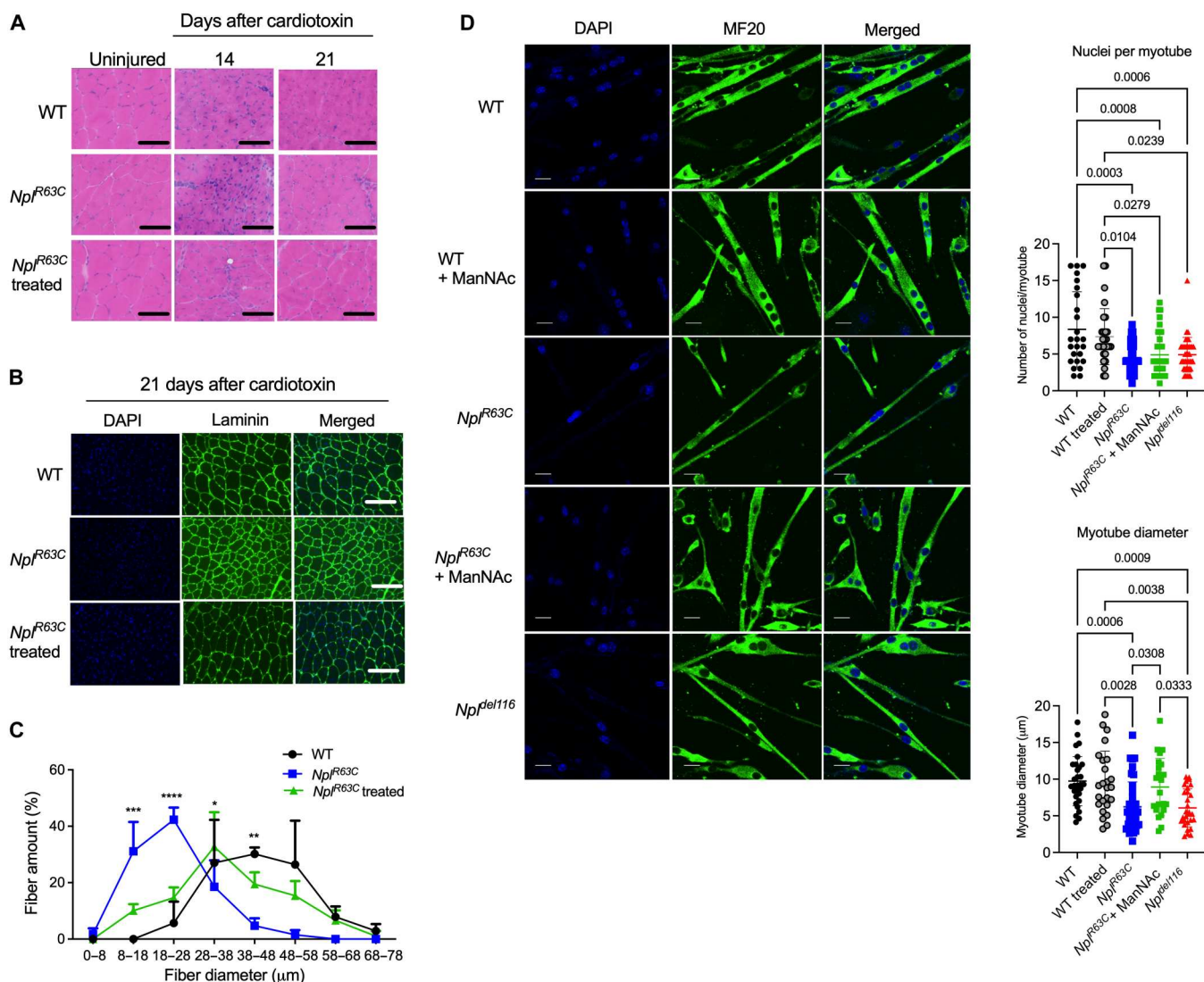
Fig. 5. ManNAc rescues deficits in muscle regeneration in *Npl^R63C* mice. (**A**) Histological changes in tibialis anterior muscle on the 14th and 21st days of regeneration after intramuscular cardiotoxin injection. Panels show representative muscle cross sections after H&E staining. Scale bar, 150 μm. Three WT, three *Npl^R63C*, and three ManNAc-treated *Npl^R63C* mice (two males/one female) were analyzed for each group. (**B**) Representative tibialis anterior sections from mice on the 21st day after injury stained with DAPI (blue) and anti-laminin antibody (green). Scale bar, 150 μm. (**C**) Distribution of myofiber diameters in mice 21 days after injury. Diameters of myofibers were quantified by morphometric analysis of tibialis anterior sections using ImageJ software. Three mice (two males/one female) were studied for each group. Statistical analyses were performed using two-way ANOVA with a Bonferroni post hoc test; *$P < 0.05$, **$P < 0.01$, ***$P < 0.001$, and ****$P < 0.0001$. (**D**) Delayed fusion of myoblasts and maturation of myotubes from *Npl^R63C* and *Npl^R63C* mice are rescued by ManNAc. Panels show representative micrographs of myogenic cells from WT, *Npl^R63C*, and *Npl^del116* mice, cultured in the absence or presence of 800 μM ManNAc, on the 5th day of differentiation into myotubes. Cells were labeled with DAPI (blue) and MF20 antibody (myosin heavy chain, green). Graphs show the number of nuclei per myotube and the diameter of myosin-positive myotubes quantified with ImageJ software. Scale bars, 20 μm. Data are presented as means ± SEM (three independent cultures were established per condition; 20 to 30 cells were analyzed for each culture). Statistical analyses were performed using a one-way ANOVA test with a Tukey post hoc test.

mice (Fig. 7B and table S1). In particular, a significant reduction in asialo-biantennary structures combined with a significant increase in disialo- and trisialo-biantennary *N*-glycans and those containing Neu5Gc was detected in MALDI profiles of glycans from *Npl^R63C* animals (Fig. 7B). The increased sialylation level of biantennary species was found associated with a significant accumulation of one individual trisialylated structure at mass/charge ratio (*m/z*) 3243.59 (A2G2Sg3), fully indicative of the glycosylation defect. Further analysis by MALDI-TOF/TOF MS/MS allowed us to

pinpoint the location of the NeuGc moieties of the trisialylated biantennary ion at *m/z* 3243.59, corresponding to the glycan that is specifically increased in *Npl^R63C* mouse muscles. The fragmentation spectrum (Fig. 7C) showed intense B/Y ion pairs (*16*) at *m/z* 877.4/2389.4 and 1268.6/1998.1, consistent with a monosialylated sequence Neu5Gc-Gal-GlcNAc at one branch and with a disialo-antenna Neu5Gc₂-Gal-GlcNAc at the other branch, respectively. The presence of the BZ ions for the internal fragments at *m/z* 374.2 and 641.3, in turn, suggested existence of a disubstituted
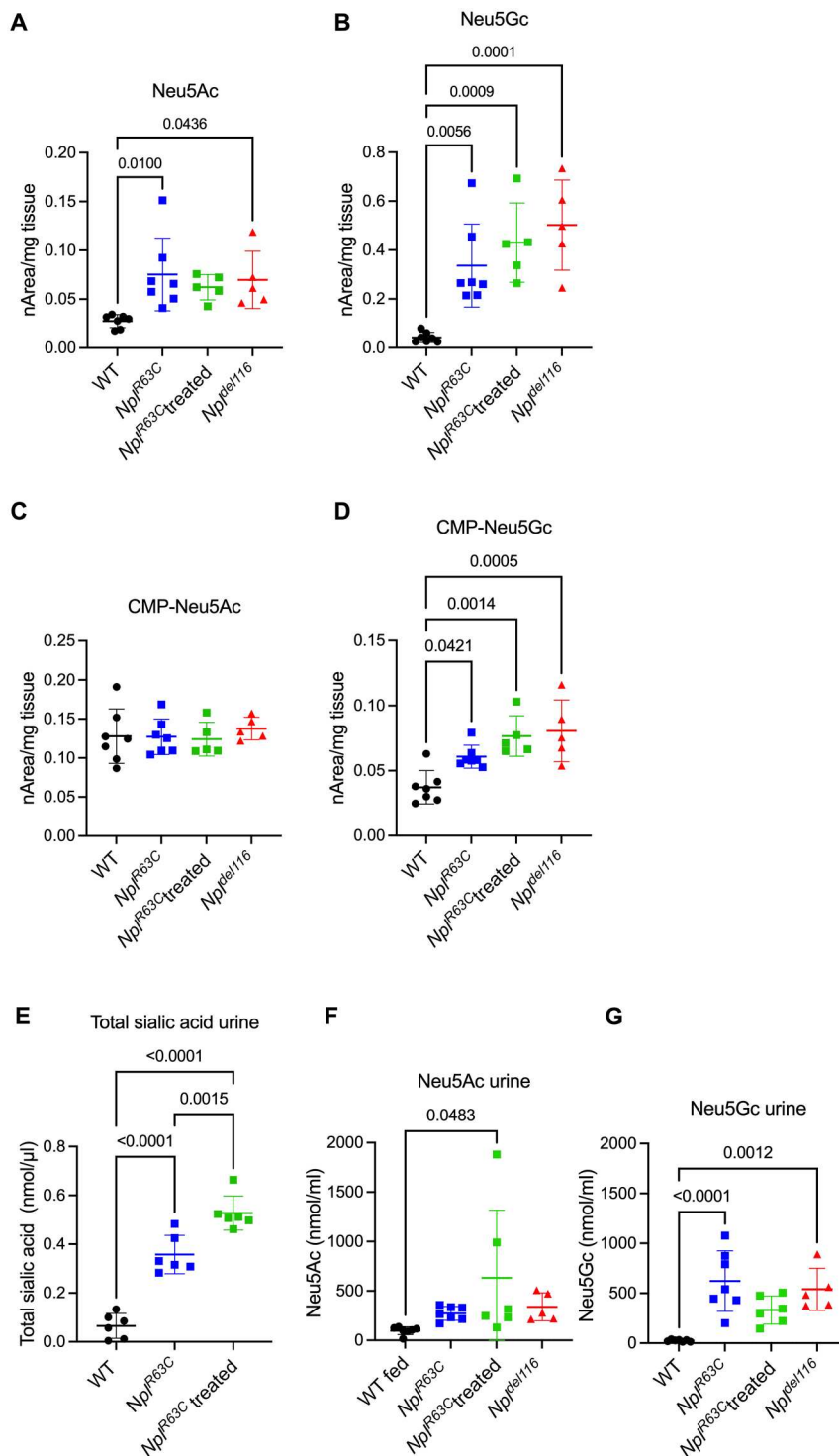
Fig. 6. Metabolites of Sia synthesis pathway are elevated in NPL-deficient mice. Levels of Neu5Ac (**A**), Neu5Gc (**B**), and Sia-nucleotides, CMP-Neu5Ac (**C**) and CMP-Neu5Gc (**D**), were measured in muscle tissues of WT, Npl^{del116}, Npl^{R63C}, and ManNAc-treated Npl^{R63C} mice. Levels of total Sia (**E**), Neu5Ac (**F**), and Neu5Gc (**G**) were measured in urine of WT, Npl^{del116}, Npl^{R63C}, and ManNAc-treated Npl^{R63C} mice. Graphs show individual values, means, and SD for the experiments performed with five to seven mice per group. Statistical analyses were performed using a one-way ANOVA test with a Tukey post hoc test.
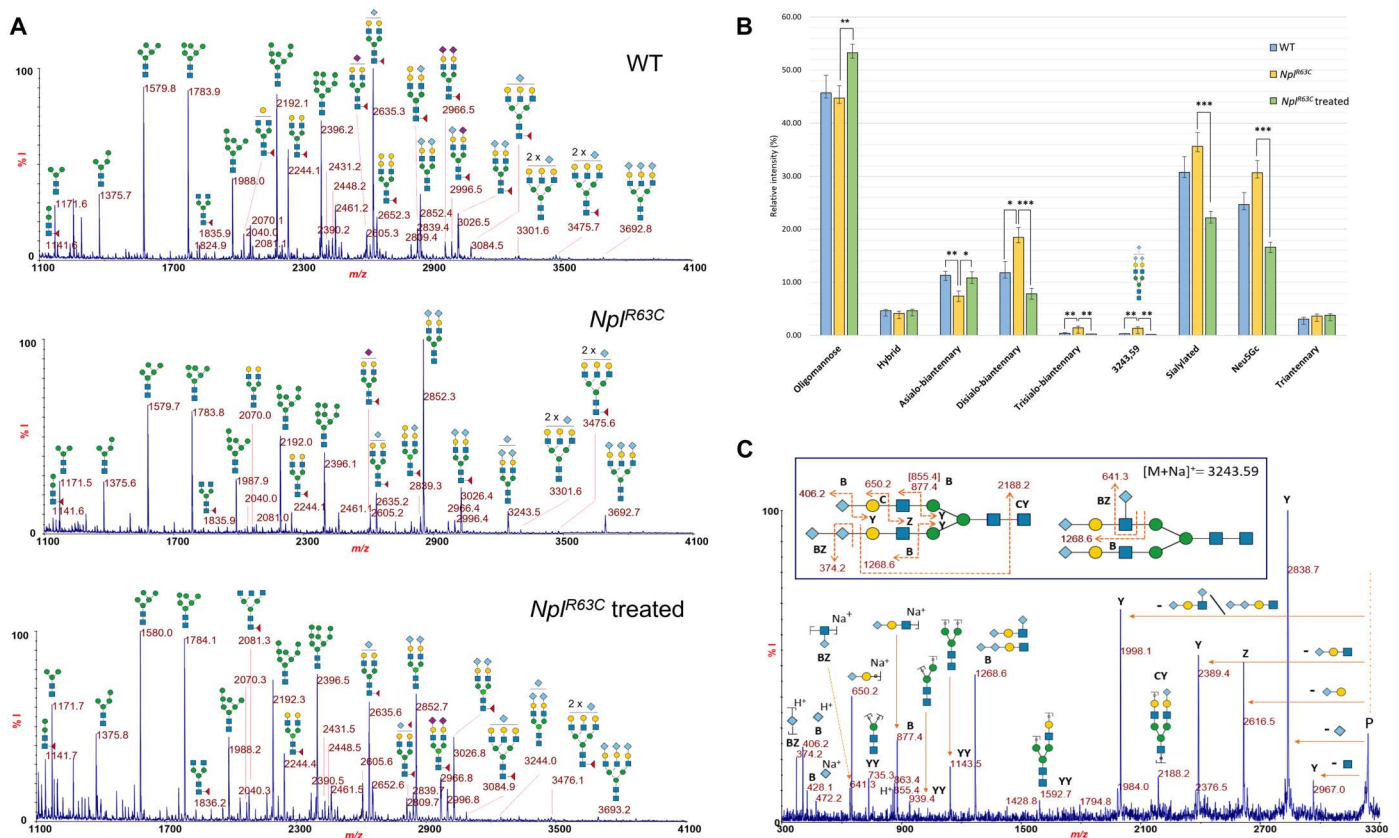
Fig. 7. Abnormal protein glycosylation in *Npl^R63C* mice. (A) MALDI-TOF profiles (mass-range between *m/z* 1100 and 4100) of permethylated *N*-glycans from muscle tissue glycoproteins representative for WT, *Npl^R63C*, and ManNAc-treated *Npl^R63C* mice samples. Species were detected as [M+Na]⁺ molecular ions (monoisotopic masses). **(B)** Comparison of the relative peak areas (shown as means ± SEM and normalized to the total areas of the 42 individual species reported in table S1) of different *N*-glycan populations from mouse muscle tissue glycoproteins in WT and NPL-mutant mice. Statistical analyses were performed using a one-way ANOVA test with a Tukey post hoc test; *$P < 0.05$, **$P < 0.01$, and ***$P < 0.001$. **(C)** MALDI-TOF/TOF analysis of the hypersialylated biantennary species at *m/z* 3243.59 that significantly accumulate in *Npl^R63C* samples and decrease after ManNAc treatment. The overall fragmentation pattern denotes the occurrence of two distinct isomers differing in the position of the extra Neu5Gc at the disialo-antenna. In all panels, graphical representation of glycans is based on the third edition of *Essentials of Glycobiology* (*59*): GlcNAc, blue square; Man, green circle; Gal, yellow circle; Neu5Ac, purple diamond; Neu5Gc, light blue diamond; Fuc, red triangle; % I, percentage of intensity

Neu5Gc, derived from the sequence Neu5Gc-Neu5Gc-Gal-GlcNAc, and a terminal Neu5Gc linked to the antennary GlcNAc, derived from the isomeric Neu5Gc-Gal-(Neu5Gc)GlcNAc epitope, demonstrating that both structures shown in Fig. 7C are present in the muscle tissues.

In *Npl^R63C* mice treated with ManNAc, normal sialylation levels were mainly restored, as revealed by the substantial increase in the asialo-biantennary glycans and corresponding decrease in disialo- and trisialo-species, including A2G2Sg3 (Fig. 7, A and B). Conversely, no significant changes in the relative amount of triantennary glycans were observed.

Because dystroglycan, a dystrophin complex component, is one of the main muscular glycoproteins, we tested whether its glycosylation is altered in the NPL-deficient mice. After posttranslational modification, dystroglycan precursor is cleaved into two subunits—the extracellular α-dystroglycan (α-DG) and the transmembrane β-DG (*17*). Association of these two subunits creates a link between the actin cytoskeleton and the extracellular matrix. Since glycosylation of α-DG is critical for its attachment to extracellular matrix proteins, congenital defects in O-mannosyl–linked glycan chains of this protein lead to multiple muscle dystrophies collectively

known as α-dystroglycanopathy (*18*). The levels of α-DG in the tissues of WT, *Npl^del116*-, *Npl^R63C*-, and *Npl^R63C*-treated mice, analyzed by immunoblotting with IIH6C4 monoclonal antibody specific to glycosylated epitopes on α-DG, were similar. However, when α-DG from muscle extracts of WT, *Npl^del116*-, *Npl^R63C*-, and ManNAc-treated *Npl^R63C* mice was purified by immunoprecipitation and analyzed by immunoblotting with *Sambucus nigra* lectin (SNL), which preferentially binds Sia attached to terminal galactose in α-2,6 and, to a lesser degree, α-2,3 linkage, we found an increase of SNL staining in *Npl^del116* and *Npl^R63C* mice, consistent with increased sialylation and a reduction of SNL staining in treated *Npl^R63C* mice (Fig. 8A).

Since TEM analysis of muscle tissue revealed structural mitochondrial abnormalities, we also explored potential changes in glycosylation of mitochondrial proteins. Mitochondria were isolated from mouse muscles by differential centrifugation and analyzed by blotting with SNL. While most protein bands showed similar lectin staining in samples from WT and NPL-deficient mice, we observed an increased sialylation of a 130- to 140-kDa protein in both *Npl^del116* and *Npl^R63C* mouse tissues (Fig. 8B). Increased SNL
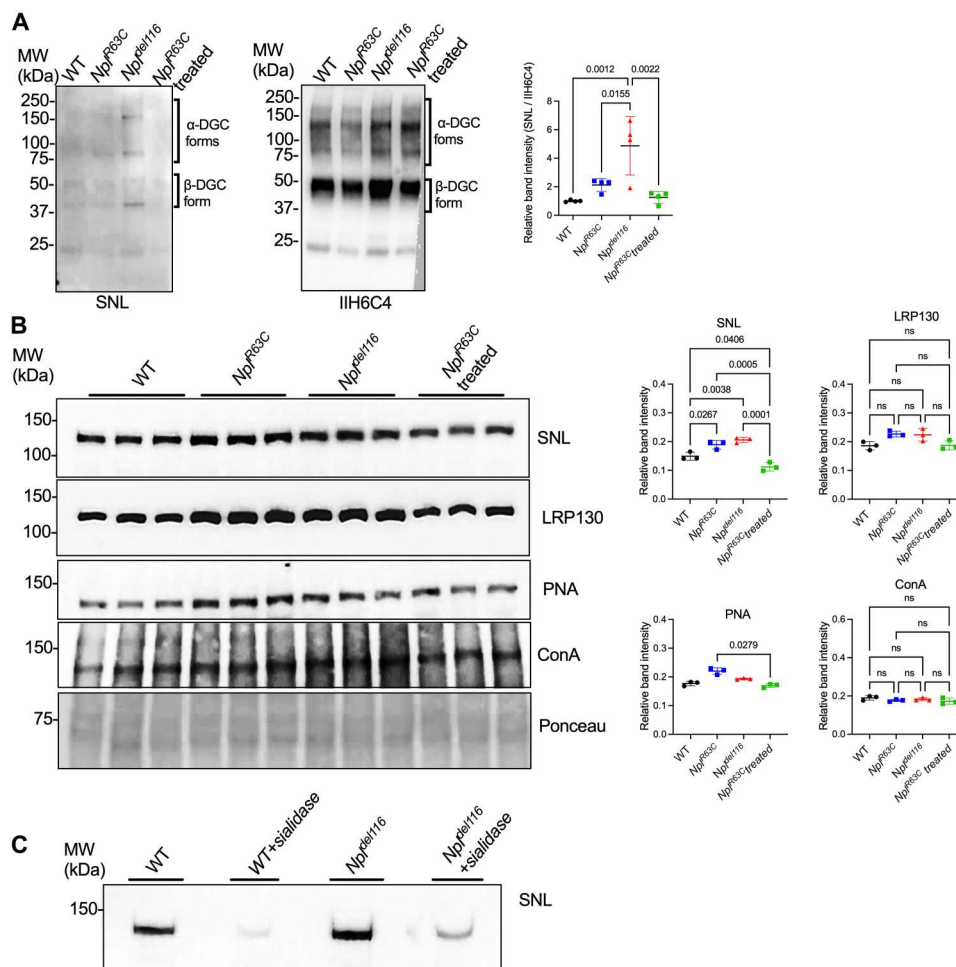
Fig. 8. Increased sialylation of α-DG and mitochondrial LRP130 in the muscle tissues of *Npl^R63C* mice is restored by ManNAc treatment. (**A**) α-DG from muscle extracts of WT, *Npl^del116*, *Npl^R63C*, and ManNAc-treated *Npl^R63C* mice was purified by immunoprecipitation and analyzed by blotting with anti–α-DG antibody, clone IIH6C4 (right) and SNL (left). Graph shows combined intensities (individual values, means, and SD) of α-DG bands, labeled with SNL, and normalized by combined intensities of α-DG bands, labeled with IIH6C4 antibodies. Equal protein loading was verified by Ponceau staining. Four mice per group were analyzed. (**B**) Proteins in the mitochondria homogenates, purified from muscles of WT, *Npl^R63C*, *Npl^R63C*, and ManNAc-treated *Npl^del116* mice, were analyzed by blotting with SNL lectin, anti-LRP130 antibodies, PNA lectin, and ConA lectin. Graphs show intensities (individual values, means, and SD) of protein bands, labeled with lectins or antibodies, and normalized by total protein abundance measured by Ponceau staining. Three mice per group were analyzed. (**C**) Mitochondrial protein homogenates from WT and *Npl^del116* mice, treated or not, by bacterial pan-specific sialidase were analyzed by SNL lectin. Treatment drastically reduced the affinity of LRP130 protein band to SNL. All statistical analyses were performed using a one-way ANOVA test with a Tukey post hoc test.

staining of this protein was rescued in mitochondrial extracts from muscles of ManNAc-treated *Npl^R63C* mice (Fig. 8B).

On the immunoblot, the 130- to 140-kDa protein band was recognized with antibodies against mitochondrial leucine-rich pentatricopeptide repeat motif-containing protein (LRP130) (Fig. 8C). LRP130 is an mRNA binding protein involved in regulation of oxidative phosphorylation (OXPHOS) and control of mitochondrial gene expression (*19*). LRP130 also showed affinity to peanut agglutinin (PNA), specific for O-linked β-galactose residues and concanavalin A (ConA), specific for mannose residues (Fig. 8, C to E). However, only the intensity of SNL-stained band was increased in NPL-deficient mice and further decreased in ManNAc-treated *Npl^R63C* mice, suggesting changes in Sia residues but not in whole glycans. When the samples were pretreated with exogenous

bacterial sialidase before blotting, the LRP130 band lost an affinity to SNL, demonstrating specificity of staining.

NPL is essential for maintenance of mitochondrial function and muscle energy production

The second group of metabolites increased in muscle tissues of NPL-deficient mice consisting of key metabolites of the glycolysis pathway or pathways downstream of glycolysis, including glucose, fructose-1 phosphate, β-alanine, lactate, and pyruvate. In *Npl^R63C* mice receiving the ManNAc treatment, the levels of all above metabolites were similar to those in WT mice (fig. S6).

The increase in pyruvate level in NPL-deficient mice was counterintuitive. Since NPL catalyzes cleavage of Sia into ManNAc and pyruvate, reduced pyruvate levels were expected in the muscles of NPL-deficient mice. We hypothesized that elevated levels of

pyruvate in muscle could be an indication of induced glycolysis resulting from deficient energy production by OXPHOS. If OXPHOS is impaired or reduced, pyruvate is converted into lactate and further into β-alanine. To validate this hypothesis, we measured levels of lactate, pyruvate, and activities of several enzymes of the Krebs cycle in the quadriceps tissues of WT, Npl^{del116}, and untreated and treated Npl^{R63C} mice by biochemical assays. The levels of lactate and pyruvate in tissues of Npl^{del116} and Npl^{R63C} mice were increased and normalized in treated Npl^{R63C} mice compared to WT (Fig. 9, A and B). At the same time, no significant differences in activities of Krebs cycle enzymes, lactate dehydrogenase, pyruvate dehydrogenase, oxoglutarate dehydrogenase, glutamate pyruvate transaminase, and glutamate oxaloacetate transaminase were detected in muscle homogenates from WT, Npl^{del116}, and Npl^{R63C} mice (fig.

S7). Protein levels of cytochrome c oxidase subunit 4 (COX4), measured by immunoblotting, were increased in the total protein extracts from quadriceps tissues of Npl^{del116} and Npl^{R63C} mice compared with WT mice (Fig. 9C). However, when COX4 protein levels were measured in purified mitochondria from quadriceps tissues (20), no significant difference was observed between Npl^{del116}, Npl^{R63C}, and WT mice (Fig. 9D), suggesting that the increased COX4 levels in total muscle protein extracts reflected a higher number of mitochondria in muscles of NPL-deficient animals. Krebs cycle metabolites such as malic acid and succinate were also present at higher levels in NPL-deficient Npl^{del116} and Npl^{R63C} mice, consistent with increased number of mitochondria in their muscle cells, while adenosine triphosphate (ATP) levels were similar (fig. S6). Last, drastically increased number of
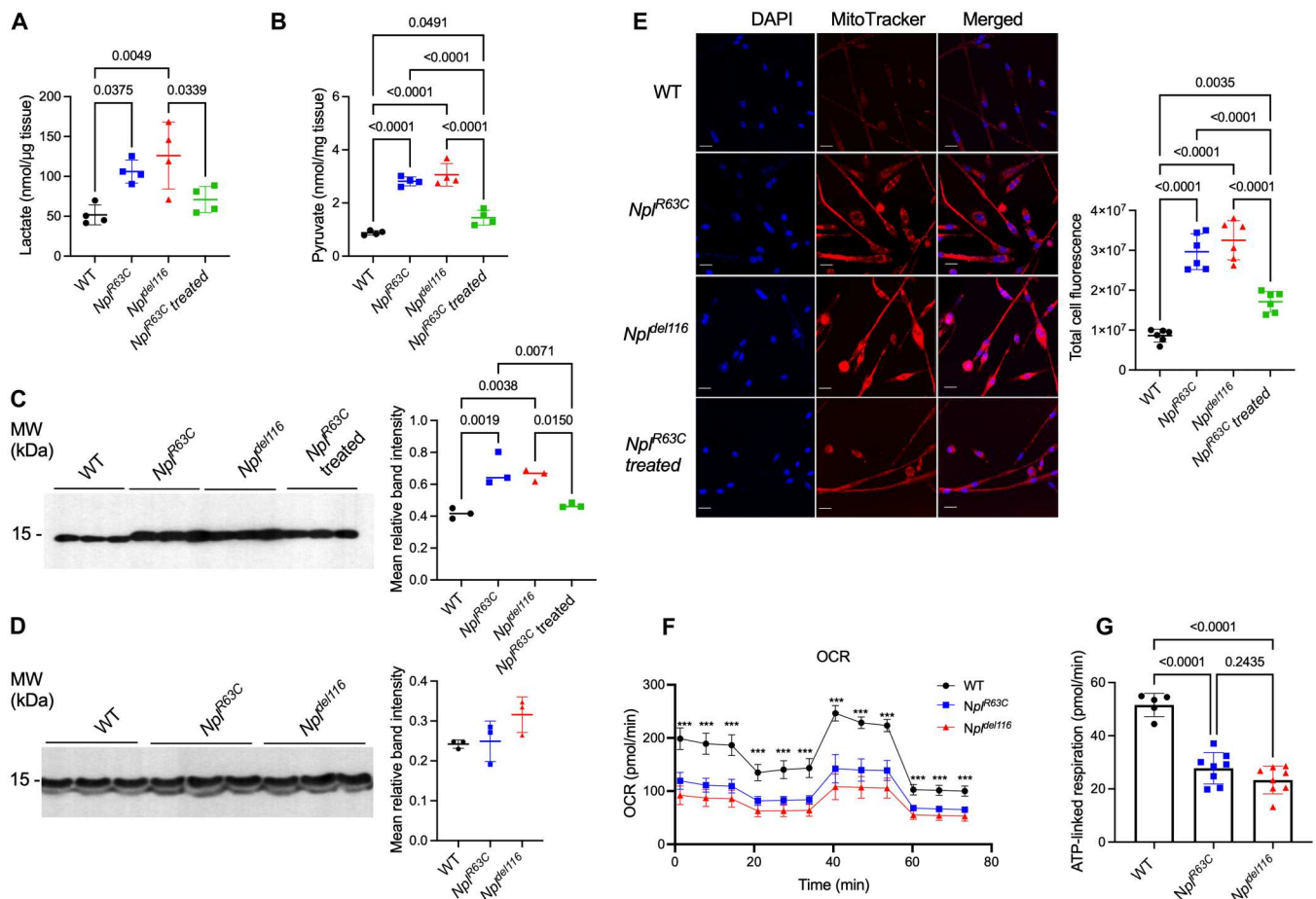
Fig. 9. Mitochondrial abnormalities in the muscles and myoblasts of NPL-deficient mice. Increased lactate (**A**) and pyruvate (**B**) in quadriceps of WT, Npl^{R63C}, and Npl^{del116} but not of ManNAc-treated Npl^{R63C} mice. $N = 4$ (2 males/2 females per group). (**C**) Immunoblot (left) shows increased COX4 protein in quadriceps muscles of WT, Npl^{R63C}, and Npl^{del116} but not of ManNAc-treated Npl^{R63C} mice. Quantification of COX4 band intensities (right) normalized by total protein. Individual values, means, and SD of experiments with three mice per group are shown. Statistical analyses were performed using a one-way ANOVA test with a Tukey post hoc test. (**D**) Immunoblot (left) shows similar levels of COX4 in purified mitochondria from muscles of WT, Npl^{R63C}, and Npl^{del116} mice. Quantification of COX4 band intensities (right) normalized by total protein abundance. Individual values, means, and SD of experiments with three mice per group are shown. (**E**) Increased abundance of mitochondria in myotubes of NPL-deficient mice. Fluorescent microscopy images (left) of primary myoblast-derived myotubes of WT, Npl^{R63C}-, Npl^{del116}-, and Npl^{R63C}-treated mice on day 3 of differentiation, labeled with DAPI and MitoTracker. Scale bars, 20 μm. Quantification of MitoTracker fluorescence (right) performed with ImageJ. Individual data, means, and SD of the experiments with cells from six cultures per group. Reduced oxygen consumption rate (**F**) and ATP-linked respiration (**G**) in cultured primary myoblasts of Npl^{R63C} and Npl^{del116} mice are detected using the XFe-24 Extracellular Flux Analyzer. Graphs show means and SD of three experiments performed with individual cell cultures from three mice per group. Statistical analyses were performed using ANOVA test with a Tukey post hoc test (A) to (E) and two-way ANOVA test with Bonferroni post hoc test (F), ***$P < 0.0001$ (WT versus NPL-deficient mice).

mitochondria in myotubes produced from cultured myoblasts from Npl^{del116} and Npl^{R63C} mice was demonstrated by MitoTracker Deep Red FM staining (Fig. 9E). When myotubes were cultured in the presence of 800 µM ManNAc in the differentiation medium, the levels of mitochondria were partially normalized (Fig. 9E). Together, these results indicated that muscle tissues of NPL-deficient mice present alterations in glycolysis and OXPHOS pathways.

To access mitochondrial function and glycolysis flux directly, we used XFe-96 Extracellular Flux Analyzer to measure the oxygen consumption rate (OCR), an indicator of mitochondrial respiration, in cultured primary myoblasts derived from WT and NPL-deficient mice. Compared with the WT cells, primary myoblasts derived from NPL-deficient mice showed significantly reduced rate for the mitochondrial respiration (Fig. 9F) and ATP-linked respiration (Fig. 9G). Other OCR-related parameters, such as basal respiration, maximal respiration, ATP production, proton leak, and reserve capacity, were also reduced (fig. S8). Together, these results strongly suggest that in the NPL-deficient mice, the energy production is compromised and relies mainly on glycolysis.

Last, to test the hypothesis that alterations in muscle energy production caused by NPL deficiency could also lead to muscle dysfunction, we compared endurance of fed WT and Npl^{R63C} mice and mice challenged by a 12-hour fasting using an accelerated rotarod test. We did not observe a significant difference in latency to fall between fed and starved WT mice. However, starved Npl^{R63C} mice were significantly less performant on rotarod than fed Npl^{R63C} mice, consistent with increased fatigue (Fig. 10A). As expected, both fed and starved Npl^{R63C} mice had significantly lower latency to fall compared with their WT counterparts. We then collected urine from WT and Npl^{R63C} fed and fasted mice to measure urinary excretion of Neu5Ac and Neu5Gc by LC-MS/MS. Both Neu5Ac and Neu5Gc were drastically increased in fasted and fed Npl^{R63C} mice compared with their WT counterparts, although Neu5Gc showed a higher increase (~50-fold) compared to Neu5Ac (~4-fold) (Fig. 10, B and C). These data are consistent with our previous results (13) demonstrating that the recombinant human NPL enzyme with Arg63Cys variant retained some residual activity against Neu5Ac. In contrast, no activity was detected against Neu5Gc. Unlike in the WT mice, the levels of Neu5Ac and Neu5Gc in the urine of Npl^{R63C} mice were further increased after fasting, and, again, this effect was more pronounced for Neu5Gc (Fig. 10, B and C). The changes in the levels of Neu5Ac and Neu5Gc in the muscles of fed and fasted WT and Npl^{R63C} mice (Fig. 10, D and E) generally recapitulated changes in the urine, with Neu5Gc showing drastic increase in fed Npl^{R63C} mice, compared to fed WT mice, and in fasted Npl^{R63C} mice, compared to fed Npl^{R63C} mice. Analysis of CMP-Neu5Ac (Fig. 10F) showed relatively unaltered levels, while levels of CMP-Neu5Gc were elevated in fed Npl^{R63C} mice compared to WT mice and in fasted Npl^{R63C} mice compared to fed Npl^{R63C} mice (Fig. 10G). Together, these results suggest that the rate of NPL-catalyzed cleavage of Sia increases upon fasting. NPL activity in the muscles of WT mice was also significantly increased after fasting (Fig. 10H). In fasted WT mice, we also could detect a similar increase in the catalytic activity of neuraminidase 2 (NEU2), the neuraminidase isoenzyme most abundant in the muscle, localized in the cytoplasm and active at neutral pH (Fig. 10I). It is tempting to speculate that in the normal muscle, starvation increases production of free Sia and its turnover into ManNAc and pyruvate, the latter potentially used for an additional energy production. In contrast, in the muscle of Npl^{R63C} mice, free Sia are partially excreted and partially recycled for production of sialoglycans, in agreement with the higher levels of CMP-Neu5Gc and Neu5Gc in fasted compared to fed NPL-deficient mice. Interestingly, 10 days after cardiotoxin-induced injury, both NPL and NEU2 activities in the muscle are also increased more than twofold (Fig. 10, J and K), suggesting that the same pathway is also activated during the muscle regeneration. To further explore this hypothesis, we assessed the expression levels of Npl in publicly available datasets of single-cell RNA sequencing experiments performed on skeletal muscle at different points during developmental myogenesis and adult muscle regeneration (fig. S9). Analysis of Npl mRNA levels during muscle regeneration in adult mice was performed on a dataset (21) that studied cells at different time points after a myotoxin injury (0.5, 2, 3.5, 5, 10, and 21 days after injury). Npl showed a peak of expression (~15% of cells expressing high Npl levels) at 5 days after injury, a time point at which myoblasts enter differentiation and initiate fusion. To investigate Npl expression in muscle development, we used a dataset in which cells were collected at different time points (10 days, 21 days, 5 months, 24 months, and 30 months postnatal) (22). At the early time points (10 and 21 days postnatal), the muscles are still in an active state of developmental myogenesis. The Npl expression was higher at the earliest time point (10 days postnatal) but remained at much lower levels than in regenerating muscles, with only ~2% of cells expressing high Npl levels. We also analyzed similar data for development of human muscles at different point during embryogenesis (23) and determined that NPL was only expressed at a constant and low levels and in a small proportion (~1%) of cells, with a small peak at 7 to 8 weeks of gestation. Overall, analysis of these datasets is coherent with our observation that NPL activity is predominantly up-regulated during muscle regeneration.

To test this further, we measured NPL and NEU2 activities in quadriceps muscle tissues from two mouse models of muscular dystrophy, mdx and DMSXL mice. Mdx mouse is a model of Duchenne muscular dystrophy with a point mutation in exon 23 of the DMD gene, leading to the lack of expression of the dystrophin protein (24). The absence of dystrophin induces muscle degeneration, chronic inflammation, and fibrosis of muscle tissue (24). DMSXL mouse, a mouse model of myotonic dystrophy type 1, carries a 45-kb human genomic fragment containing the mutant $DMPK$ gene with >1000 CTG repeats. Transcription of the mutant $DMPK$ allele leads to the accumulation of toxic mRNA, resulting in the formation of nuclear foci, impaired alternative splicing, and disrupted mRNA translation and stability contributing to disease progression. DMSXL mice experience growth delay, muscle atrophy, and weakness (25). For both models, the tissues of 8- to10-week-old mice, homozygous for the mutant allele, were compared with age- and sex-matching WT mice with the same genetic background (C57Bl/10 for mdx and C57Bl/6 for DMSXL mice).

In muscle homogenates of both mouse models, we found drastically increased NPL activity, compared to their WT siblings (Fig. 10L), suggesting that up-regulation of free Sia degradation pathway can be a general biomarker of muscle injury and muscle dystrophy. NEU2 activity was significantly increased in the muscles of mdx mice and showed a nonsignificant trend for increase in the muscles of DMSXL mice (Fig. 10M). Last, we analyzed NPL and NEU2 activities in the fresh-frozen muscle biopsy of a
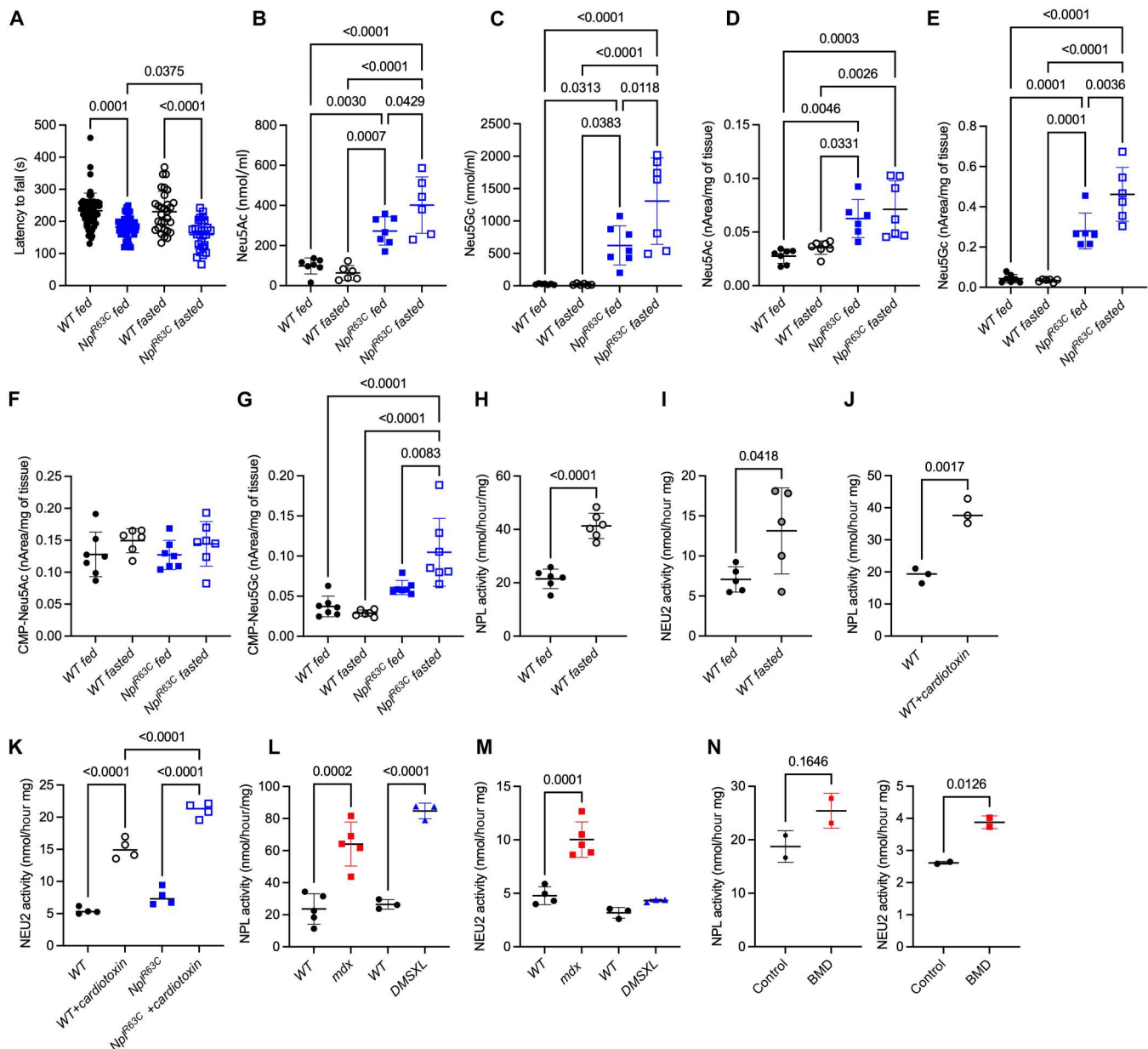
Fig. 10. Starvation, muscle injury, and muscle dystrophy induce NPL-catalyzed Sia cleavage. (**A**) Fasting reduces latency to fall for NpI^{R63C} but not for WT mice in accelerated rotarod test. $N = 16$ (8 males/8 females) mice per group. (**B**) Neu5Ac and (**C**) Neu5Gc are increased in the urine of fasted NpI^{R63C} but not fasted WT mice. $N = 7$ (4 males/3 females) per group. (**D** and **E**) Neu5Gc in the quadriceps muscle of NpI^{R63C} mice, but not of WT mice, is increased by fasting. (**F** and **G**) Fasting increases levels of CMP-Neu5Gc, but not of CMP-Neu5Ac, in the quadriceps muscle of NpI^{R63C} mice. $N = 7$ (4 males/3 females) mice per group. (**H** and **I**) Fasting increases NPL and NEU2 activities in quadriceps muscles from WT. $N = 6$ (3 males/3 females) mice per group. (**J** and **K**) NPL and NEU2 activities are increased in homogenates of tibialis anterior muscle 10 days after injection of cardiotoxin. $N = 4$ (2 males/2 females) mice per group. (**L** and **M**) NPL and NEU2 activities are increased in homogenates of tibialis anterior muscle tissues from Duchenne's muscular dystrophy, mdx, and a myotonic dystrophy type 1, DMXL, mouse models compared with their respective WT controls. $N = 5$ (2 males/3 females) mice per group for mdx mice and their controls, and 3 males for DMXL mice and their controls. (**N**) NPL activity shows a trend toward an increase, and NEU2 activity is increased in homogenates of quadriceps muscle biopsies of a patient affected with BMD compared with age-/sex-matched nonmyopathic control. Individual results, means, and SD of technical replicas are shown. Statistical analysis was performed using a two-way ANOVA with a Bonferonni post hoc test (A), one-way ANOVA with a Tukey post hoc test (B) to (H) and (K), and t test (H) to (J) and (L) to (N).

patient affected with Becker muscular dystrophy (BMD), an X-linked recessive inherited disorder characterized by slowly progressive proximal weakness. The patient was homozygous for the pathogenic *DYS* c.3940C>T variant resulting in a premature termination codon. The age-/sex-matched control had a histologically normal muscle biopsy performed for a clinical suspicion of mitochondrial disease. We found that NEU2 activity was significantly increased in the tissue homogenate of the BMD patient, while NPL showed a trend for about 20% increase compared with the normal muscle (Fig. 10N).

DISCUSSION

Previously, we have identified genetic variants in the *NPL* gene in two siblings with cardiomyopathy/skeletal muscle myopathy and demonstrated that these variants interfere with NPL protein levels and/or enzymatic activity. We have also demonstrated that *npl* zebrafish morphants develop muscle and heart phenotypes that are rescued by the induced expression of the WT enzyme, but not by its p.Arg63Cys or p.Asn45Asp variants, establishing association of these mutations with the disease.

In the current work, we show that NPL plays an essential role in muscle development and function by regulating glycoprotein sialylation and energy metabolism. Homozygous mice expressing the patient-derived Npl Arg63Cys variant, which reduces NPL protein and activity in tissues to the levels below detection, as well as mice homozygous for the deleterious 116-bp deletion in *Npl* exon 4 show structural muscular defects, reduction of maximal muscle force, increased muscle fatigue, and low endurance. Npl^{R63C} mice have somewhat milder phenotype and a trend of lower levels of Sia in the urine, suggesting that a small portion of NPL escapes the degradation in the endoplasmic reticulum and its activity is responsible for partial cleavage of Sia. Although our enzymatic assay was not sensitive enough to confirm or to reject this hypothesis, it is consistent with the results of our previous study (13) where we detected human Arg63Cys NPL protein overexpressed in HEK293 cells. NPL deficiency also affects adult muscle regeneration. Muscle regeneration after the cardiotoxin-induced injury in Npl^{R63C} mouse is significantly impaired, the formation of new myotubes is delayed, the number of centrally located nuclei is increased, and newly formed fibers have a smaller diameter. Although the diameter of fibers was similar between the WT and NPL-deficient mice in the absence of cardiotoxin challenge, analysis of muscle by TEM reveals multiple structural defects, including abnormal and disarrayed fibers, as well as myocytes with uneven shape and size presenting increased number of mitochondria. These structural defects were found in both knock-in Npl^{R63C} and knock-out Npl^{del116} animals, demonstrating the association with NPL deficiency.

Unexpectedly, heart function in Npl^{R63C} mice was normal according to the echography results. Further work is necessary to explain the mechanism behind the discrepancy between the mouse and human/zebrafish phenotypes; however, it could be potentially related to the fact that relative NPL expression levels in the mouse heart are negligible in comparison with those detected in the fish or humans (26, 27). Besides, we cannot exclude the possibility that mice challenged by systemic injections of cardiotoxin or physical stress could develop cardiomyopathy with a lower threshold than the WT mice.

At the molecular level, we have observed an increase in disialo- and trisialo-biantennary *N*-glycans in the muscles of Npl^{R63C} mice. These glycans mainly contained Neu5Gc. Free Neu5Gc levels remained below detection levels in the muscle tissues and urine of WT mice but were drastically increased in NPL-deficient animals, providing evidence that NPL is exclusively responsible for cleavage of Neu5Gc in muscle cells. Since high levels of CMP-Neu5Gc were observed in the muscles of both Npl^{R63C} and Npl^{del116} mice, we propose that in the absence of NPL, Neu5Gc is reused for the synthesis of CMP-Neu5Gc that further results in appearance of glycan chains with abnormally increased *N*-glycolyl-sialylation. Although the conversion of CMP-Neu5Ac into CMP-Neu5Gc by cytosolic CMP-Neu5Ac hydroxylase (CMAH) was thought to be the major source of this metabolite in animal tissues (28), there is a genetic evidence that Neu5Gc can be directly used for the synthesis of CMP-Neu5Gc. CMAH is evolutionary inactivated in humans; however, Neu5Gc has been found in glycoconjugates on the cell surface of human tissues (14, 16) and is likely derived from the consumption of animal products, such as red meat and milk (17, 29–31). It has been reported that these processes can cause autoimmune reactions and result in chronic inflammation (32). Our previous data have shown that both R63C and N45D mutations, identified in the human patients, completely abolish the enzymatic activity toward Neu5Gc, suggesting that NPL deficiency could also result in increased incorporation of both Neu5Gc and Neu5Ac into the protein glycan chains in human muscles (13).

Previous works have established that abnormal (either hypo- or hyper-) glycosylation of α-DG disrupts binding of dystrophin-associated glycoprotein complex to extracellular matrix, causing structural rearrangements and muscular dystrophies (33, 34). Since our present data revealed increased incorporation of Neu5Gc in protein *N*-glycans, we directly analyzed sialylation of α-DG and found that it was increased in the muscle tissues of NPL-deficient mice. However, because our previous studies have shown that Sia content in glycan chains is not crucial for laminin-binding activity of α-DG, which mainly depends on *O*-mannosylation of the proteins (9), further experiments are necessary to determine whether α-DG function is altered in NPL-deficient mice.

Another protein, where sialylation is increased in NPL-deficient mice and rescued by ManNAc treatment, is the mitochondrial matrix protein LRP130 involved in the regulation of OXPHOS and the maintenance of basal mitochondrial phenotype in human skeletal muscles (35). LRP130 is particularly highly expressed in the liver (36), where it plays an essential role in induction of mitochondrial gene expression in response to fasting (37). LRP130 has four potential N-linked glycosylation sites and binds the wheat germ agglutinin, which specifically recognizes Neu5Ac and GlcNAc glycans (38); however, according to our knowledge, the current study is the first one to demonstrate changes in its sialylation.

Previous studies have demonstrated that LRP130, heavily acetylated on Lys residues, is deacetylated by sirtuin 3 (SIRT3) in response to fasting, promoting a mitochondrial transcriptional program that enhances hepatic OXPHOS (37). We speculate that in tissues of NPL-deficient mice, increased sialylation of LRP130 may interfere with its deacetylation and activation, but further studies are necessary to verify this.

Paradoxically, both hypersialylation of α-DG and LRP130 and defects in muscle structure and regeneration in NPL-deficient mice are reversed by a dietary supplementation with ManNAc, a

precursor of Neu5Ac synthesis. Since this metabolite is converted to Neu5Ac by consequent actions of GNE, NANS, and NANP, ManNAc treatment is known to increase protein sialylation reduced in GNE myopathy (*39*) and in minimal change disease (MCD) [reviewed in (*40*)]. At this point, we cannot provide a mechanistic explanation why ManNAc reduces hypersialylation of selected proteins, including α-DG and LRP130, associated with NPL deficiency.

It is tempting to speculate that NPL deficiency results in the reduced ability to degrade Neu5Gc and its enrichment in glycan chains, which can modify their properties. In turn, ManNAc stimulates endogenous production of Neu5Ac and CMP-Neu5Ac, pushing the equilibrium back toward a normal distribution between 5-glycolyl and 5-acetyl derivatives of Sia in the treated *Npl*^R63C mice.

In addition to structural defects, muscles of NPL-deficient mice reveal alterations in the energy metabolism pathways, including induced glycolytic flux and reduced rates of OXPHOS, resembling the Warburg effect [see (*41*) for a recent review]. These alterations, leading to increased levels of glycolytic metabolites such as pyruvate, lactate, malate, succinate, fructose 1-phosphate, and others, as well as of the number of apparently dysfunctional mitochondria in myotubes, can be the cause of reduced endurance of NPL-deficient mice challenged by fasting and exercise. Since all these parameters are normalized by ManNAc treatment, we speculate that they reflect secondary compensatory changes in the muscle triggered in response to abnormal glycosylation and structural defects, including those in myotubes and mitochondria.

At the same time, since Sia biogenesis is derived from glucose metabolism, we cannot exclude a possibility that metabolites of the Sia pathway may directly influence glycolysis and OXPHOS through yet-to-be-discovered regulatory feedback loops. NPL enzyme shows highest expression levels in the kidney and colon and is present at high levels in the liver and skeletal muscles, i.e., the organs actively involved in gluconeogenesis that produces glucose to supply glucose-dependent cells during starvation. Levels of NPL and the upstream enzyme NEU2, which potentially generates free Sia in the muscles, are increased during fasting, indirectly supporting the hypothesis that these enzymes can also be involved in regulation of gluconeogenesis. They are similarly increased after the muscle injury or in the dystrophic muscle of mdx/DMSXL mouse models and BMD patient, suggesting the importance of elimination of free Sia by NPL in muscle regeneration process. Notably, the recent study in the constitutive *Neu2* knockout mice reported increased sialylation of proteins involved in muscle function and decreased sialylation of proteins involved in lipid metabolism (*42*). However, we also cannot exclude the possibility that ManNAc itself has a positive effect on the mitochondrial health and improves abnormalities in the OXPHOS regulation by a yet-to-be-discovered mechanism.

Together, our results provide evidence that NPL plays an essential role in muscle function, especially during muscle regeneration, by controlling the levels of free Sia and sialylation of muscle glycoproteins. These results are highly coherent with the expression pattern of the gene during muscle regeneration, mouse development, and human gestation (*21*–*23*). Moreover, induced production and NPL-catalyzed cleavage of free Sia may represent a general biomarker of injured or dystrophic muscle. Our results also demonstrate that chronic treatment with ManNAc rescues aberrant protein glycosylation and restores muscle strength and regeneration process to the levels observed in the WT mice. ManNAc has been shown to be well tolerated by humans up to the dose of up to 0.2 g kg^{-1} BW day^{-1} (*43*). It is accepted that in mice this dose corresponds to 1 g kg^{-1} BW day^{-1}, which was used in our study. Moreover, oral ManNAc is currently being tested in several clinical trials for the inherited metabolic defects of sialylation associated with GNE myopathy (*39*) and MCD (*40*), and preliminary reports indicate that the treatment is safe and restores defects in protein sialylation. Both diseases were also effectively treated by oral ManNAc in the corresponding mouse models (*44*–*46*). The absence of pronounced cardiac phenotype in mice did not allow us to test whether cardiomyopathy could also be ameliorated by ManNAc treatment. However, this is likely considering our previous results in the zebrafish embryos, where the drug rescued heart edema in the *npl* knockdown embryos.

MATERIALS AND METHODS
Study approval
All animal experiments were approved by the Animal Care and Use Committee of Centre Hospitalier Universitaire (CHU) Ste-Justine Research Centre (approval numbers 2020-2668 and 2021-3213) in accordance with the Canadian Council on Animal Care guidelines. Ethical approval for the research involving human tissues was granted by Research Ethics Board of CHU Ste-Justine. Fresh-frozen muscle samples, collected for diagnostic purposes from a patient with BMD and from an age-matched patient with a normal biopsy, were provided by the Neuromax biobank of CHU Ste-Justine together with clinical descriptions and results of genetic analysis. The collection of samples was performed for diagnostic purposes, and the patients consented to donate the excessive tissues to the muscle biobank of CHU Ste-Justine for research purposes.

Murine models
A knock-in *Npl*^R63C C57BL/6 mouse strain, carrying human missense mutation Arg63Cys, and a knockout *Npl*^del116 strain, with a 116-bp deletion in exon 4 of the *Mus musculus N-acetylneuraminate lyase* (*Npl*) gene, were generated at McGill Integrated Core for Animal Modeling using CRISPR-Cas9 technology. To generate knock-in and knockout founders, a single-guide nucleotide RNA (sgRNA) was designed, using the CRISPR guide design tools (https://zlab.bio/resources), to target a genomic site on the murine *Npl* locus with minimal potential off-target effects. sgRNA and Cas9 mRNA were microinjected into zygotes with single-stranded oligodeoxynucleotide (ssODN), barring a c.270C>T mutation encoding for the R63C change (100 ng/μl of ssODN, 20 ng/μl of sgRNA, and 20 ng/μl of Cas9; fig. S1). After overnight culture, two-cell zygotes were transferred into surrogate mothers, and pups were delivered at full term. At weaning, pups were genotyped by Sanger sequencing of single-allele fragments obtained by PCR amplification of genomic DNA from the tail clips. The founder mice were bred to C57BL/6n mice to generate F1 heterozygous animals. To test for the presence of potential off-target effects, the sgRNA sequence (TGAACGTCGCCAGGTCGCGG) was blasted against the *M. musculus* genome. The 800-bp fragments around top three matches in exon sequences, presenting the highest identity score, were amplified by PCR from genomic DNA of F1

founders followed by Sanger sequencing to analyze for the presence of deleterious variants. The mice were further backcrossed to C57BL/6n mice for three generations to segregate and eliminate potential off-target changes in other alleles. The progenies were intercrossed to generate WT, heterozygous, and homozygous mutant (*Npl^{R63C}* and *Npl^{del116}*) animals.

Mice were housed in an enriched environment with continuous access to food and water, under constant temperature and humidity, on a 12:12-hour light:dark cycle and were bred as heterozygous pairs. Mouse genotyping was performed on tail genomic DNA, extracted using standard protocols. PCR amplifications were performed across the c.270C>T mutation with genomic DNA as template, using the primer set 5′-TCCCATCTGTCCCTAATGGC-3′ and 5′-CTGCTCTGCCTCCCCTTAGT-3′ and the following PCR program: 94°C for 4 min, 35 cycles (94°C for 30 s, 60°C for 30 s, and 72°C for 2 min), and 72°C for 10 min. Since the c.270C>T mutation eliminated the *Hpy99I* restriction site, to distinguish between mutant and WT amplicons, the amplified PCR fragment was digested with *Hpy99I* (New England Biolabs, catalog no. R0615S) at 37°C for 1 hour and then separated on a 2% agarose gel. Fragments of 454 and 309 bp were detected for the WT allele, and an undigested 763-bp fragment for the targeted *Npl^{R63C}* allele. To genotype *Npl^{del116}* progeny, the amplification product was separated on a 2% agarose gel, where a 647-bp band was detected for the *Npl^{del116}* allele.

Mdx mice (C57BL/10ScSn-*Dmd^{mdx}*/J) (24) were obtained from The Jackson Laboratory (strain no. 001801). DMSXL mice (25) were provided by G. Gourdon. Mice of both strains were housed under 12:12-hour light:dark cycle at 21°C and 40% humidity in pathogen-free cages.

NPL activity assay in mouse tissues

WT, *Npl^{R63C}*, and *Npl^{del116}* 2-month-old mice were anesthetized with isoflurane and sacrificed by cervical dislocation. Tissues from skeletal muscles, visceral organs, and brain were harvested, snap-frozen with liquid nitrogen, and kept at −80°C until further analysis. Frozen tissue (100 mg) was homogenized in 250 μl of deionized water in 1.5-ml Eppendorf tubes using a sonic dismembrator (Artek Systems Corporation). NPL enzymatic activity in the homogenate was measured against Neu5Ac (Sigma-Aldrich, catalog no. A0812), as previously described (47). The concentration of the product, ManNAc, was determined as described previously by Reissig *et al.* (48). Protein concentration in the homogenate was measured using Bradford assay (Thermo Fisher Scientific, catalog no. 23225).

Quantitative RT-PCR

Npl mRNA level in the kidney tissues was measured by reverse transcription (RT)–qPCR using the LightCycler 96 apparatus (Roche Life Science). Total RNA was isolated from tissues using TRIzol reagent (Invitrogen), and its quality and concentration were assessed by spectrophotometry using the NanoDrop apparatus (Thermo Fisher Scientific, Wilmington, DE, USA). Total RNA (1 μg) was subjected to RT using the iScript cDNA synthesis kit (Bio-Rad, Hercules, CA, USA). RT-qPCR was performed in triplicate for each sample using SYBR Green Supermix (Bio-Rad, Hercules, CA, USA) for 40 cycles with a three-step program (20 s of denaturation at 95°C, 30 s of annealing at 58°C, and 30 s of extension at 72°C) and the primer set 5′-CCACCATCACTCCAAT

GACA-3′ and 5′-CCCTTGGTTAACCCATTCCT-3′. Amplification specificity was assessed with a melting curve analysis. The fold-change expression was determined by the comparative cycle threshold (CT) method ($2^{-\Delta\Delta CT}$) and normalized to the housekeeping gene *PRL32*.

Immunoblotting, lectin blotting, and immunoprecipitation

Frozen mouse muscle tissues (100 mg) were homogenized in 250 μl of radioimmunoprecipitation assay buffer (50 mM tris-HCl, 150 mM NaCl, 1% Nonidet P-40, 0.25% Na-deoxycholate, 0.1% SDS, and 2 mM EDTA) supplemented with protease and phosphatase inhibitor cocktail (Roche) using a sonic dismembrator (Artek Systems Corporation). The homogenate was cleared by centrifugation at 13,000*g* for 10 min, and the protein concentration in the supernatant was quantified using the Bradford reagent (Bio-Rad). To test specificity of SNL blotting, protein lysates were treated with exogenous sialidase from *Arthrobacter ureafaciens* (Sigma-Aldrich, 10269611001) according to the manufacturer's protocol.

After separation by SDS–polyacrylamide gel electrophoresis on an 8% gel, the proteins were transferred to a nitrocellulose membrane and hybridized with polyclonal rabbit anti-NPL antibodies (1:2000, Abcam, catalog no. ab223521), mouse anti–α-DG antibody clone IIH6C4 (1:2000, Millipore Sigma), monoclonal mouse anti–β-actin antibody (1:1000, Santa Cruz Biotechnology, catalog no. SC-47778), polyclonal rabbit anti-LRPPRC antibody (1:2000, Thermo Fisher Scientific, catalog no. 21175-1-AP), biotinylated *S. nigra* lectin (1:5000, Vector Laboratories, catalog no. B-1305-2), PNA lectin (1:1000, Vector Laboratories, catalog no. B-1075-5), or ConA lectin (1:5000, Vector Laboratories, catalog no. B-1005-5) followed by horseradish peroxidase (HRP)–conjugated anti-mouse immunoglobulin G (IgG) and anti-rabbit IgG secondary antibodies (Cell Signaling Technology, 1:8000 and 1:10,000, respectively) or streptavidin-HRP (1:10,000, GE Healthcare). The membrane was developed with Pierce ECL Western blotting substrate (Thermo Fisher Scientific), and the signal was detected using the G:Box Chemi XQR system (Syngene). For immunoprecipitation, 500 μl of the protein extract was supplemented with mouse anti–α-DG antibody clone IIH6C4 (1:100, Sigma-Aldrich, catalog no. 05-593) and 35 μl of Protein A/G Sepharose beads (Abcam, ab193262). After incubation and washing, antigen elution was performed according to the manufacturer's protocol.

Measurement of metabolites in mouse urine and tissues

Urine was collected overnight using metabolic cages. Free Sia (Neu5Ac and Neu5Gc combined) were measured using a colorimetric/fluorometric assay kit (BioVision) according to the manufacturer's instructions. Concentrations of lactate and pyruvate in homogenates of skeletal muscle tissues were measured using L-lactate assay kit (Abcam) and pyruvate assay kit (BioVision), respectively, according to the manufacturer's protocol. To conduct untargeted metabolic profiling of muscle tissues, metabolites were extracted with methanol/water (1:1) and analyzed with reversed-phase UPLC-MS/MS on the SYNAPT XS instrument as described (15). From these data, levels of CMP-Sia and glycolysis metabolites were extracted as normalized relative intensities. Individual levels of Neu5Ac and Neu5Gc in urine were determined by LC-MS/MS essentially as described using 1,2,3-$^{13}C_3$-Neu5Ac as internal standard (IS) (49). Briefly, urine samples were diluted five times in MilliQ water, spiked with IS (1:1) and 2% formic acid (20:1). Separation

of samples by LC was obtained using an Atlantis 3-μm dC18 column (2.1 mm × 100 mm) with mobile phase A, 0.3% formic acid in MilliQ water, and B, 100% methanol. A linear elution gradient of 99.9 to 50% of mobile phase A was used (1 to 1.1 min), followed by isocratic elution with 50% A (1.1 to 4.0 min) and finally equilibration with 99.9% mobile phase A (4.0 to 5.9 min). The flow rate was 0.25 ml/min from 0.0 to 2.5 min and 0.28 ml/min from 2.51 to 5.9 min. The elution profiles were monitored by a Xevo TQ-S micro mass spectrometer in negative ion mode with MS/MS transitions for Neu5Ac: 308/87; Neu5Gc: 324/87; and IS: 311/90. For data analysis, raw peak areas were normalized on the IS and quantified on the basis of a calibration curve (1 to 100 μM) for Neu5Ac and Neu5Gc. For measurements in muscle tissue, mouse quadriceps samples were homogenized in 75 mM ammonium carbonate buffer (pH 7.4), and $1,2,3\text{-}^{13}C_3\text{-}Neu5Ac$ was added as IS to each replicate before metabolite extraction. Equal amounts of tissue homogenate were used for extraction with methanol:acetonitrile (1:1). CMP-Neu5Ac and CMP-Neu5Gc were measured using triethylamine ion-pairing buffer, while Neu5Ac and Neu5Gc levels were measured using tributylamine ion-pairing buffer, as described previously (50). CMP-Neu5Ac and CMP-Neu5Gc values were normalized for the summed levels of guanosine diphosphate (GDP)–mannose, GDP-fucose, uridine diphosphate (UDP)–galactose, UDP−N-acetylhexosamine, UDP−glucuronic acid, UDP-xylose, and cytidine diphosphate (CDP)–ribitol, while Neu5Ac and Neu5Gc values were normalized using the IS.

Analysis of isometric contractile properties of a muscle

Before the measurements, the mice were injected intraperitoneally with buprenorphine (0.1 mg/kg BW) and anesthetized with sodium pentobarbital (50 mg/kg BW) 15 min after. The EDL muscles were carefully dissected, attached to an electrode and a force sensor (300C dual-mode lever, Aurora Scientific, Canada), and incubated at 25°C in buffered physiological saline solution [Krebs-Ringer solution: 137 mM NaCl, 5 mM KCl, 2 mM $CaCl_2$, 24.7 mM $NaHCO_3$, 2 mM $MgSO_4$, 1.75 mM NaH_2PO_4 (pH 7.4)], supplemented with dextrose (2 mg/ml) and carbogen (95% O_2, 5% CO_2) to allow the viability of muscle fibers. Optimal muscle length (L_o) was determined and gradually adjusted until the maximum isometric twitch tension was achieved, at which point the muscles were allowed a 10-min equilibration in the bath before the contractile measurement. A force-frequency curve was established by stimulating the muscles at different frequencies, ranging from 10 to 150 Hz, with 2-min rest between stimulations. Thereafter, muscle length and weight were measured to assess specific muscle force (N/cm^2). To do so, mathematical approximation of cross-sectional area was calculated on the basis of the following formula: force (N) × fiber length (0.44 × L_o for the EDL muscle) × muscle density (1.06 g/cm^3)/muscle mass (g). After conducting the titanic force measurements, EDL muscles rested for an additional 2 min before undergoing a 5-min fatigue resistance protocol. The fatigue protocol consisted of 60 consecutive stimulus trains at 40 Hz of frequency, with each pulse lasting for 1 s and applied every 5 s.

Grip strength test

The test was performed on 10-week-old WT, Npl^{R63C}, and Npl^{R63C} mice, treated or not with ManNAc. The grip strength of mouse paws was measured using a grip strength meter (Bioseb, Pinellas Park, FL, USA) as follows. Mice were allowed to grip the metal bar with their front paws, while suspended from their tails in the position perpendicular to the bar, and subsequently dragged by pulling their tails parallel to the bar until breaking the grasp. The test was repeated three times, and the best trial was used for analysis. The grip strength data were recorded in g-force units and normalized for body weight.

Front limb and hindlimb suspension tests

Front limb and hindlimb suspension tests were performed on WT, Npl^{R63C}, and Npl^{del116} mice. The front limb suspension test was used to measure the arm and paw strength of 6-week-old mice. First, mice were allowed to grasp a wire strung across a stable object and hang from the wire with both forepaws. The testing area was placed over a padded drop zone. Then, the mice were held firmly by the body and enabled to grasp the wire with both forepaws. The time of recording was started with the release of the mouse and stopped with the fall. The test was repeated for a total of three times. Hindlimb suspension was used to determine hindlimb strength in 10-day-old mice essentially as described (51). A standard 50-ml plastic conical tube was padded with laboratory wipes. The pups were gently placed, face down, into the tube with their hind legs hanging over the rim. The time until the fall of the mouse was recorded. The test was repeated for a total of three times.

Rotarod test

Mice either fed the normal diet or fasted for 16 hours were placed on an automated rotarod (Ugo Basile) with an accelerating speed ranging from 4 to 40 rpm. The time to fall was recorded in three test trials.

Cardiotoxin-induced muscle injury

Intramuscular injections of cardiotoxin (Latoxan, 10 μM solution in saline, 50 μl per mouse), a myotoxin frequently used to induce a severe and uniform muscle injury (52), were performed into the right tibialis anterior muscle under general anesthesia. Mice were anesthetized with isoflurane and sacrificed by cervical dislocation, and the tibialis anterior muscle was harvested on the 14th or 21st day after injury. Muscle samples were embedded in optimal cutting temperature compound, frozen in isopentane (2-methylbutane, Sigma-Aldrich), cooled with liquid nitrogen, and cryosectioned in 10-μm-thick slices. Cross sections were stained with hematoxylin and eosin (Sigma-Aldrich), and microphotographs were acquired using axioscan (Zeiss Axio Scan.Z1). Alternatively, cross sections were used for immunochemical analysis as described below.

Immunohistochemistry

Muscle cross sections were washed once with phosphate-buffered saline (PBS) and fixed in 2% paraformaldehyde for 10 min, permeabilized with 0.1% Triton X-100/0.15 M glycine/PBS for 10 min, and extensively washed with PBS. Samples were further blocked using 5% goat serum and 2% bovine serum albumin in PBS at room temperature for 2 hours. Rabbit anti-myogenin (1:1000, catalog no. ab124800, Abcam) and rabbit anti-laminin (1:1000, catalog no. ab1157, Abcam) primary antibodies diluted in blocking solution were applied at 4°C overnight. Samples were washed extensively with PBS, and secondary antibodies (anti-rabbit IgG antibody coupled with Alexa Fluor 488, 1:1000, Thermo Fisher Scientific) were applied in blocking solution for 1 hour at room temperature.

Following washes with PBS, the sections were counterstained with 4′,6-diamidino-2-phenylindole (DAPI) for 10 min and mounted with Permafluor (Thermo Fisher Scientific). Slides were analyzed, and images were taken using an epifluorescence microscope (EVOS M500 Imaging System) with appropriate filters or SP8-DLS inverted confocal microscope (Leica TCS SP8). Fiber diameter was calculated using ImageJ software.

ManNAc treatment

Npl^{R63C} breeding mouse pairs and nursing females were administered with water supplemented with 5 mg/ml (~1.0 g kg^{-1} BW day^{-1}) or 1 mg/ml (~0.2 g kg^{-1} BW day^{-1}) of ManNAc (Goldbio). The solution was changed twice a week. After weaning at 21 days, the offspring continued to be treated with the same dose of ManNAc until the time of analysis (44).

Echocardiography

Transthoracic echocardiography was performed at 7 months using an instrument to measure rodent cardiac function (VisualSonics Vevo3100, VisualSonics, Toronto, ON, Canada). Anesthesia was induced by putting the mouse in an induction chamber with a flow of 3% isoflurane/100% oxygen at 1 liter/min for 1 to 2 min. Once an animal lost its righting reflex, it was placed supine on a heated platform with its nose enveloped in a nosecone to keep the mouse anesthetized by 2% isoflurane. M mode images were recorded when the heart rate of the mice was maintained at 450 to 500 beats per minute. LVEF, LVEDD, and LVESD were also measured (53).

Analysis of N-linked protein glycans

Mouse muscle tissue was homogenized and lysed in a chloroform/methanol/water mixture 4:8:3 (v/v/v), as described previously (54). The protein pellet was separated from the lipid-containing supernatant by centrifugation and cleaned by repeated washes with acetone/water (4:1) at 4°C. The final pellet was dried under a stream of nitrogen and stored at −20°C until the analysis. For N-glycan analysis, ~2 mg of each protein sample was resuspended in 0.2 ml of 0.1% RapiGest Surfactant (Waters Corporation, Milford, MA) in 50 mM NH_4HCO_3 with the aid of an ultrasonic processor equipped with a 2-mm probe (130 W, 50% amplitude, 5 min in pulsing mode). The obtained homogenate was incubated at 100°C for 5 min, followed by reduction in 5 mM dithiothreitol (Sigma-Aldrich) at 56°C for 30 min and alkylation in 15 mM iodoacetamide (Sigma-Aldrich) in the dark at room temperature for 45 min. Glycan chains were cleaved by peptide-N-glycosidase F (4 U; Roche Molecular Biochemicals, Mannheim, Germany) overnight at 37°C. The released N-glycans were purified and permethylated by ICH_3 in a dimethyl sulfoxide/NaOH slurry, as described (55, 56). MALDI-TOF and MALDI-TOF/TOF analyses of permethylated N-glycans were performed using 5-chloro-2-mercaptobenzothiazole (10 mg/ml in 80:20 methanol/water, v/v) as matrix and acquired on a 4800 proteomic analyzer (AB Sciex) in positive polarity and in reflector mode (55). Data were analyzed using Data-Explorer 4.9 software. Glycan structures were assigned on the basis of molecular weight, knowledge of the biosynthetic pathway, and MS/MS analyses using the bioinformatic tools developed by the Consortium for Functional Glycomics (http://functionalglycomics.org). Tissues of three animals were analyzed for each group. Statistical analyses were performed using PASW Statistic 18, and P values were calculated by analysis of variance (ANOVA) with a Tukey post hoc test.

Activity assays of Krebs cycle enzymes

The enzymatic activities of Krebs cycle enzymes, lactate dehydrogenase, pyruvate dehydrogenase, oxoglutarate dehydrogenase, glutamate pyruvate transaminase, and glutamate oxaloacetate transaminase were measured in total homogenates of quadriceps muscles from 2-month-old WT, Npl^{del116}, and Npl^{R63C} mice, as previously described (57).

Isolation and differentiation of muscle satellite cells

Isolation and differentiation of satellite cells from hindlimb muscles of 2-month-old WT, Npl^{R63C}, and Npl^{del116} mice were performed as described (58). Briefly, muscles were finely dissected with scissors, minced, and enzymatically digested with collagenase/dispase (Sigma-Aldrich) for 45 min at 37°C. The digested muscle was passed through a 40-μm cell strainer and then centrifuged to collect the cell pellet, which was resuspended in Dulbecco's modified Eagle's medium (DMEM) with 10% fetal bovine serum (FBS). The satellite cells were purified from cell suspension by consecutively preplating cells in plastic dishes and collecting nonadherent cells. Myoblasts were expanded on collagen-coated petri dishes with proliferating medium: Ham's F10 medium (Gibco), 20% FBS (Wisent), 1% penicillin-streptomycin (Gibco), and fibroblast growth factor 2 (2.5 ng/ml; Wisent). Myoblasts were differentiated in low-serum medium (50% Ham's F10, 50% DMEM low glucose, 1% penicillin-streptomycin, and 5% horse serum) for 4 days. Immunofluorescence was performed for myogenin (clone EPR4789, 1:500, Abcam) and myosin heavy chain (clone MF20, 1:20, Developmental Studies Hybridoma Bank), and the fusion index was measured as the proportion of total nuclei located in multinucleated myotubes. The levels of mitochondria were estimated in myotubes stained with MitoTracker Deep Red FM (Thermo Fisher Scientific, catalog no., M22426) according to the manufacturer's protocol.

Transmission electron microscopy

Animals were anesthetized with sodium pentobarbital and perfused with PBS followed by 5% glutaraldehyde in 0.1 M phosphate buffer (pH 7.0). Muscles were removed and immersed overnight in 5% glutaraldehyde at 4°C. Samples were trimmed and washed with 0.1 M cacodylate buffer (pH 7.4) before secondary fixation with 1% osmium tetroxide and 1.5% potassium ferrocyanide for 2 hours. Samples were dehydrated with a gradient ethanol series and propylene oxide, infiltrated with epoxy resin, and embedded in a Durcupan-Epon mixture. Semi-thin sections were cut, stained with toluidine blue, and examined on light microscope (Leica). Regions of interest for electron microscopy were selected, and ultrathin sections were cut, mounted on 200 mesh copper grids, and analyzed by a TEM using Tecnai G2 Spirit BioTwin instrument.

Oxygen consumption rate

OCR was measured using a Seahorse Xfe96 instrument and analyzed with Wave 2.6.0 software (Agilent Technologies). Primary myoblasts were seeded in collagen-coated 96-well plates at a density of 20,000 cells per well and cultured for 2 days in full growth medium. One hour before OCR measurements, cells were incubated in MitoStress test assay medium: DMEM 5030 with 2.5

mM glucose (Sigma-Aldrich, catalog no. G7528-250G), 0.5 mM carnitine (Sigma-Aldrich, catalog no. C0158-5G), and 5 mM Hepes (pH 7.4) (Wisent). Oligomycin (2 μM) (Sigma-Aldrich, catalog no. O4876), 400 nM carbonyl cyanide-*p*-trifluoromethoxy-phenyl-hydrazon (Abcam, catalog no. ab120081), and 10 nM sodium pyruvate (Gibco, catalog no. 11360070), followed by 1 μM antimycin A (Sigma-Aldrich, catalog no. A8674), were injected sequentially to cell medium while OCR was measured.

Statistical analysis

For data collection and analysis, the experimenter was blinded to the identity of the sample. All experiments were repeated independently at least twice in the laboratory with similar results. Statistical analyses were performed using Prism GraphPad 9.3.0 software (GraphPad Software, San Diego, CA). The normality for all data was checked using the D'Agostino and Pearson omnibus normality test. Significance of the difference was determined using *t* test when comparing two groups and one-way ANOVA test, followed by Tukey's multiple comparison test when comparing more than two groups. Two-way ANOVA followed by Bonferroni or Tukey's post hoc tests was used for two-factor analysis. A *P* value of 0.05 or less was considered significant.

Supplementary Materials

This PDF file includes:
Figs. S1 to S10
Table S1

REFERENCES AND NOTES

1. A. Varki, Sialic acids in human health and disease. *Trends Mol. Med.* **14**, 351–360 (2008).

2. S. J. Moons, G. J. Adema, M. T. Derks, T. J. Boltje, C. Büll, Sialic acid glycoengineering using N-acetylmannosamine and sialic acid analogs. *Glycobiology* **29**, 433–445 (2019).

3. H. H. Freeze, G. W. Hart, R. L. Schnaar, Glycosylation precursors, in *Essentials of Glycobiology*, A. Varki, R. D. Cummings, J. D. Esko, P. Stanley, G. W. Hart, M. Aebi, A. G. Darvill, T. Kinoshita, N. H. Packer, J. H. Prestegard, R. L. Schnaar, P. H. Seeberger, Eds. (Cold Spring Harbor Laboratory Press, 2015), pp. 51–63.

4. A. Varki, R. L. Schnaar, R. Schauer, Sialic acids and other nonulosonic acids, in *Essentials of Glycobiology*, A. Varki, R. D. Cummings, J. D. Esko, P. Stanley, G. W. Hart, M. Aebi, A. G. Darvill, T. Kinoshita, N. H. Packer, J. H. Prestegard, R. L. Schnaar, P. H. Seeberger, Eds. (Cold Spring Harbor Laboratory Press, 2015), pp. 179–195.

5. O. Pogoryelova, J. A. González Coraspe, N. Nikolenko, H. Lochmüller, A. Roos, GNE myopathy: From clinics and genetics to pathology and research strategies. *Orphanet J. Rare Dis.* **13**, 70 (2018).

6. C. D. M. van Karnebeek, L. Bonafé, X. Y. Wen, M. Tarailo-Graovac, S. Balzano, B. Royer-Bertrand, A. Ashikov, L. Garavelli, I. Mammi, L. Turolla, C. Breen, D. Donnai, V. Cormier-Daire, D. Heron, G. Nishimura, S. Uchikawa, B. Campos-Xavier, A. Rossi, T. Hennet, K. Brand-Arzamendi, J. Rozmus, K. Harshman, B. J. Stevenson, E. Girardi, G. Superti-Furga, T. Dewan, A. Collingridge, J. Halparin, C. J. Ross, M. I. Van Allen, A. Rossi, U. F. Engelke, L. A. Kluijtmans, E. van der Heeft, H. Renkema, A. de Brouwer, K. Huijben, F. Zijlstra, T. Heise, T. Boltje, W. W. Wasserman, C. Rivolta, S. Unger, D. J. Lefeber, R. A. Wevers, A. Superti-Furga, NANS-mediated synthesis of sialic acid is required for brain and skeletal development. *Nat. Genet.* **48**, 777–784 (2016).

7. M. Mohamed, A. Ashikov, M. Guillard, J. H. Robben, S. Schmidt, B. van den Heuvel, A. P. de Brouwer, R. Gerardy-Schahn, P. M. Deen, R. A. Wevers, D. J. Lefeber, E. Morava, Intellectual disability and bleeding diathesis due to deficient CMP--sialic acid transport. *Neurology* **81**, 681–687 (2013).

8. B. G. Ng, C. G. Asteggiano, M. Kircher, K. J. Buckingham, K. Raymond, D. A. Nickerson, J. Shendure, M. J. Bamshad; University of Washington Center for Mendelian Genomics, M. Ensslen, H. H. Freeze, Encephalopathy caused by novel mutations in the CMP-sialic acid transporter, SLC35A1. *Am. J. Med. Genet. A* **173**, 2906–2911 (2017).

9. M. Riemersma, J. Sandrock, T. J. Boltje, C. Bull, T. Heise, A. Ashikov, G. J. Adema, H. van Bokhoven, D. J. Lefeber, Disease mutations in CMP-sialic acid transporter *SLC35A1* result in

10. D. Kreuzmann, R. Horstkorte, G. Kohla, C. Kannicht, D. Bennmann, A. Thate, K. Bork, Increased polysialylation of the neural cell adhesion molecule in a transgenic mouse model of Sialuria. *Chembiochem* **18**, 1188–1193 (2017).

11. D. Adams, M. Wasserstein, Free sialic acid storage disorders, in *GeneReviews(®)*, M. P. Adam, H. H. Ardinger, R. A. Pagon, S. E. Wallace, L. J. H. Bean, K. Stephens, A. Amemiya, Eds. (University of Washington, 1993).

12. N. Carrillo, M. C. Malicdan, M. Huizing, GNE Myopathy: Etiology, diagnosis, and therapeutic challenges. *Neurotherapeutics* **15**, 900–914 (2018).

13. X. Y. Wen, M. Tarailo-Graovac, K. Brand-Arzamendi, A. Willems, B. Rakic, K. Huijben, A. Da Silva, X. Pan, S. El-Rass, R. Ng, K. Selby, A. M. Philip, J. Yun, X. C. Ye, C. J. Ross, A. M. Lehman, F. Zijlstra, N. Abu Bakar, B. Drögemöller, J. Moreland, W. W. Wasserman, H. Vallance, M. van Scherpenzeel, F. Karbassi, M. Hoskings, U. Engelke, A. de Brouwer, R. A. Wevers, A. V. Pshezhetsky, C. D. van Karnebeek, D. J. Lefeber, Sialic acid catabolism by N-acetylneuraminate pyruvate lyase is essential for muscle function. *JCI Insight* **3**, e122373 (2018).

14. R. O. Stephenson, Y. Yamanaka, J. Rossant, Disorganized epithelial polarity and excess trophectoderm cell fate in preimplantation embryos lacking E-cadherin. *Development* **137**, 3383–3391 (2010).

15. E. J. Want, P. Masson, F. Michopoulos, I. D. Wilson, G. Theodoridis, R. S. Plumb, J. Shockcor, N. Loftus, E. Holmes, J. K. Nicholson, Global metabolic profiling of animal and human tissues via UPLC-MS. *Nat. Protoc.* **8**, 17–32 (2013).

16. B. Domon, C. E. Costello, A systematic nomenclature for carbohydrate fragmentations in FAB-MS/MS spectra of glycoconjugates. *Glycoconj. J.* **5**, 397–409 (1988).

17. A. Akhavan, S. N. Crivelli, M. Singh, V. R. Lingappa, J. L. Muschler, SEA domain proteolysis determines the functional composition of dystroglycan. *FASEB J.* **22**, 612–621 (2008).

18. A. Kuga, M. Kanagawa, T. Toda, Recent advances in α-dystroglycanopathy. *Brain Nerve* **63**, 1189–1195 (2011).

19. H. Islam, D. A. Hood, B. J. Gurd, Looking beyond PGC-1α: Emerging regulators of exercise-induced skeletal muscle mitochondrial biogenesis and their activation by dietary compounds. *Appl. Physiol. Nutr. Metab.* **45**, 11–23 (2020).

20. C. Frezza, S. Cipolat, L. Scorrano, Organelle isolation: Functional mitochondria from mouse liver, muscle and cultured fibroblasts. *Nat. Protoc.* **2**, 287–295 (2007).

21. S. N. Oprescu, F. Yue, J. Qiu, L. F. Brito, S. Kuang, Temporal dynamics and heterogeneity of cell populations during skeletal muscle regeneration. *iScience* **23**, 100993 (2020).

22. M. J. Petrany, C. O. Swoboda, C. Sun, K. Chetal, X. Chen, M. T. Weirauch, N. Salomonis, D. P. Millay, Single-nucleus RNA-seq identifies transcriptional heterogeneity in multinucleated skeletal myofibers. *Nat. Commun.* **11**, 6374 (2020).

23. H. Xi, J. Langerman, S. Sabri, P. Chien, C. S. Young, S. Younesi, M. Hicks, K. Gonzalez, W. Fujiwara, J. Marzi, S. Liebscher, M. Spencer, B. Van Handel, D. Evseenko, K. Schenke-Layland, K. Plath, A. D. Pyle, A human skeletal muscle atlas identifies the trajectories of stem and progenitor cells across development and from human pluripotent stem cells. *Cell Stem Cell* **27**, 158–176.e10 (2020).

24. P. Sicinski, Y. Geng, A. S. Ryder-Cook, E. A. Barnard, M. G. Darlison, P. J. Barnard, The molecular basis of muscular dystrophy in the *mdx* mouse: A point mutation. *Science* **244**, 1578–1580 (1989).

25. A. Huguet, F. Medja, A. Nicole, A. Vignaud, C. Guiraud-Dogan, A. Ferry, V. Decostre, J.-Y. Hogrel, F. Metzger, A. Hoeflich, M. Baraibar, M. Gomes-Pereira, J. Puymirat, G. Bassez, D. Furling, A. Munnich, G. Gourdon, Molecular, physiological, and motor performance defects in DMSXL mice carrying >1,000 CTG repeats from the human DM1 locus. *PLOS Genet.* **8**, e1003043 (2012).

26. Npl N-acetylneuraminate pyruvate lyase [Mus musculus (house mouse)] 2022, January 5 [Available from: https://www.ncbi.nlm.nih.gov/gene/74091.

27. NCBI, NPL N-acetylneuraminate pyruvate lyase [Homo sapiens (human)] (5 January 2022).

28. D.-N. Kwon, Y.-J. Choi, S.-G. Cho, C. Park, H.-G. Seo, H. Song, J.-H. Kim, CMP-Neu5Ac hydroxylase null mice as a model for studying metabolic disorders caused by the evolutionary loss of Neu5Gc in humans. *Biomed. Res. Int.* **2015**, 830315 (2015).

29. A. K. Bergfeld, O. M. T. Pearce, S. L. Diaz, T. Pham, A. Varki, Metabolism of vertebrate amino sugars with *N*-glycolyl groups: Elucidating the intracellular fate of the non-human sialic acid N-glycolylneuraminic acid. *J. Biol. Chem.* **287**, 28865–28881 (2012).

30. R. N. Knibbs, I. J. Goldstein, R. M. Ratcliffe, N. Shibuya, Characterization of the carbohydrate binding specificity of the leukoagglutinating lectin from Maackia amurensis. Comparison with other sialic acid-specific lectins. *J. Biol. Chem.* **266**, 83–88 (1991).

31. N. Shibuya, I. J. Goldstein, W. F. Broekaert, M. Nsimba-Lubaki, B. Peeters, W. J. Peumans, The elderberry (Sambucus nigra L.) bark lectin recognizes the Neu5Ac(alpha 2-6)Gal/GalNAc sequence. *J. Biol. Chem.* **262**, 1596–1601 (1987).

32. S. Bashir, S. L. B. Arye, E. M. Reuven, H. Yu, C. Costa, M. Galiñanes, T. Bottio, X. Chen, V. Padler-Karavani, Presentation mode of glycans affect recognition of human serum anti-Neu5Gc IgG antibodies. *Bioconjug. Chem.* **30**, 161–168 (2019).

33. X.-Y. Chen, D.-Y. Song, L. Jiang, D.-D. Tan, Y.-D. Liu, J.-Y. Liu, X.-Z. Chang, G.-G. Xing, T. Toda, H. Xiong, Phenotype and genotype study of chinese *POMT2*-related α-Dystroglycanopathy. *Front. Genet.* **12**, 692479 (2021).

34. P. Franzka, H. Henze, M. J. Jung, S. C. Schüler, S. Mittag, K. Biskup, L. Liebmann, T. Kentache, J. Morales, B. Martínez, I. Katona, T. Herrmann, A.-K. Huebner, J. C. Hennings, S. Groth, L. Gresing, R. Horstkorte, T. Marquardt, J. Weis, C. Kaether, O. M. Mutchinick, A. Ori, O. Huber, V. Blanchard, J. von Maltzahn, C. A. Hübner, GMPPA defects cause a neuromuscular disorder with α-dystroglycan hyperglycosylation. *J. Clin. Invest.* **131**, e139076 (2021).

35. H. Islam, A. Ma, A. Amato, A. Cuillerier, Y. Burelle, C. A. Simpson, J. Quadrilatero, B. J. Gurd, Fiber-specific and whole-muscle LRP130 expression in rested, exercised, and fasted human skeletal muscle. *Pflugers Arch.* **472**, 375–384 (2020).

36. N. Tsuchiya, H. Fukuda, T. Sugimura, M. Nagao, H. Nakagama, LRP130, a protein containing nine pentatricopeptide repeat motifs, interacts with a single-stranded cytosine-rich sequence of mouse hypervariable minisatellite Pc-1. *Eur. J. Biochem.* **269**, 2927–2933 (2002).

37. L. Liu, M. Nam, W. Fan, T. E. Akie, D. C. Hoaglin, G. Gao, J. F. Keaney Jr., M. P. Cooper, Nutrient sensing by the mitochondrial transcription machinery dictates oxidative phosphorylation. *J. Clin. Invest.* **124**, 768–784 (2014).

38. J. Hou, F. Wang, W. L. McKeehan, Molecular cloning and expression of the gene for a major leucine-rich protein from human hepatoblastoma cells (HepG2). *In Vitro Cell. Dev. Biol. Anim.* **30**, 111–114 (1994).

39. X. Xu, A. Q. Wang, L. L. Latham, F. Celeste, C. Ciccone, M. C. Malicdan, B. Goldspiel, P. Terse, J. Cradock, N. Yang, S. Yorke, J. C. McKew, W. A. Gahl, M. Huizing, N. Carrillo, Safety, pharmacokinetics and sialic acid production after oral administration of N-acetylmannosamine (ManNAc) to subjects with GNE myopathy. *Mol. Genet. Metab.* **122**, 126–134 (2017).

40. P. Ravani, E. Bertelli, S. Gill, G. M. Ghiggeri, Clinical trials in minimal change disease. *Nephrol. Dial. Transplant.* **32**, i7–i13 (2017).

41. P. Vaupel, G. Multhoff, Revisiting the Warburg effect: Historical dogma versus current understanding. *J. Physiol.* **599**, 1745–1757 (2021).

42. M. Oh, D.-I. Ha, C. Son, J. G. Kang, H. Hwang, S. B. Moon, M. Kim, J. Nam, J. S. Kim, S. Y. Song, Y.-S. Kim, S. Park, J. S. Yoo, J.-H. Ko, K. Park, Defect in cytosolic Neu2 sialidase abrogates lipid metabolism and impairs muscle function in vivo. *Sci. Rep.* **12**, 3216 (2022).

43. S. M. Amir, S. A. Barker, W. R. Butt, A. C. Crooke, A. G. Davies, Administration of N-acetyl-D-mannosamine to mammals. *Nature* **211**, 976–977 (1966).

44. B. Galeano, R. Klootwijk, I. Manoli, M. Sun, C. Ciccone, D. Darvish, M. F. Starost, P. M. Zerfas, V. J. Hoffmann, S. Hoogstraten-Miller, D. M. Krasnewich, W. A. Gahl, M. Huizing, Mutation in the key enzyme of sialic acid biosynthesis causes severe glomerular proteinuria and is rescued by N-acetylmannosamine. *J. Clin. Invest.* **117**, 1585–1594 (2007).

45. M. C. Malicdan, S. Noguchi, Y. Tokutomi, Y. Goto, I. Nonaka, Y. K. Hayashi, I. Nishino, Per-acetylated *N*-acetylmannosamine, a synthetic sugar molecule, efficiently rescues muscle phenotype and biochemical defects in mouse model of sialic acid-deficient myopathy. *J. Biol. Chem.* **287**, 2689–2705 (2012).

46. T. K. Niethamer, T. Yardeni, P. Leoyklang, C. Ciccone, A. Astiz-Martinez, K. Jacobs, H. M. Dorward, P. M. Zerfas, W. A. Gahl, M. Huizing, Oral monosaccharide therapies to reverse renal and muscle hyposialylation in a mouse model of GNE myopathy. *Mol. Genet. Metab.* **107**, 748–755 (2012).

47. P. Brunetti, G. W. Jourdian, S. Roseman, The sialic acids. III. Distribution and properties of animal N-acetylneuraminic aldolase acids. *J. Biol. Chem.* **237**, 2447–2453 (1962).

48. J. L. Reissig, J. L. Storminger, L. F. Leloir, A modified colorimetric method for the estimation of N-acetylamino sugars. *J. Biol. Chem.* **217**, 959–966 (1955).

49. M. van der Ham, B. H. C. M. T. Prinsen, J. G. M. Huijmans, N. G. G. M. Abeling, B. Dorland, R. Berger, T. J. de Koning, M. G. M. de Sain-van der Velden, Quantification of free and total sialic acid excretion by LC-MS/MS. *J. Chromatogr. B Analyt. Technol. Biomed. Life Sci.* **848**, 251–257 (2007).

50. M. van Scherpenzeel, F. Conte, C. Bull, A. Ashikov, E. Hermans, A. Willems, W. van Tol, E. Kragt, M. Noga, E. E. Moret, T. Heise, J. D. Langereis, E. Rossing, M. Zimmermann, M. E. Rubio-Gozalbo, M. I. de Jonge, G. J. Adema, N. Zamboni, T. Boltje, D. J. Lefeber, Dynamic tracing of sugar metabolism reveals the mechanisms of action of synthetic sugar analogs. *Glycobiology* **32**, 239–250 (2022).

51. D. N. Feather-Schussler, T. S. Ferguson, A battery of motor tests in a neonatal mouse model of cerebral palsy. *J. Vis. Exp.*, 53569 (2016).

52. G. A. Garry, M. L. Antony, D. J. Garry, Cardiotoxin induced injury and skeletal muscle regeneration. *Methods Mol. Biol.* **1460**, 61–71 (2016).

53. M. J. Litt, G. D. Okoye, D. Lark, I. Cakir, C. Moore, M. C. Barber, J. Atkinson, J. Fessel, J. Moslehi, R. D. Cone, Loss of the melanocortin-4 receptor in mice causes dilated cardiomyopathy. *eLife* **6**, e28118 (2017).

54. K. Aoki, M. Tiemeyer, The glycomics of glycan glucuronylation in Drosophila melanogaster. *Methods Enzymol.* **480**, 297–321 (2010).

55. A. Palmigiano, A. Messina, R. O. Bua, R. Barone, L. Sturiale, M. Zappia, D. Garozzo, CSF N-Glycomics using MALDI MS techniques in alzheimer's disease. *Methods Mol. Biol.* **1750**, 75–91 (2018).

56. I. Ciucanu, F. Kerek, A simple and rapid method for the permethylation of carbohydrates. *Carbohydr. Res.* **131**, 209–217 (1984).

57. A. V. Artiukhov, A. Grabarska, E. Gumbarewicz, V. A. Aleshin, T. Kahne, T. Obata, A. V. Kazantsev, N. V. Lukashev, A. Stepulak, A. R. Fernie, V. I. Bunik, Synthetic analogues of 2-oxo acids discriminate metabolic contribution of the 2-oxoglutarate and 2-oxoadipate dehydrogenases in mammalian cells and tissues. *Sci. Rep.* **10**, 1886 (2020).

58. A. Benedetti, G. Cera, D. De Meo, C. Villani, M. Bouche, B. Lozanoska-Ochser, A novel approach for the isolation and long-term expansion of pure satellite cells based on ice-cold treatment. *Skelet. Muscle* **11**, 7 (2021).

59. *Essentials of Glycobiology*, A. Varki, R. D. Cummings, J. D. Esko, P. Stanley, G. W. Hart, M. Aebi, A. G. Darvill, T. Kinoshita, N. H. Packer, J. H. Prestegard, R. L. Schnaar, P. H. Seeberger, Eds. (Cold Spring Harbor Laboratory Press, 2015).